Estimation of Dynamic Load Factors for elastic cylinders under dynamic internal pressure

Christophe Garnier, Vincent Faucher, Pierre Lamagnere

Estimation of Dynamic Load Factors for elastic cylinders under dynamic internal pressure

Christophe Garnier [a,1], Vincent Faucher [a], Pierre Lamagnère [a]

[a] CEA, DES, IRESNE, Nuclear Technology Department, Cadarache F-13108 Saint-Paul-Lez-Durance, France.

Abstract

This paper discusses the design of a cylindrical test section subjected to a dynamic internal pressure for severe accident experiments performed at CEA. A commonly used method consists in computing the static equivalent response of the structure and then applying DLF coefficients. In this paper, Dynamic Load Factor (DLF) coefficients are obtained for cylinders.

Based on a cylinder subjected to a stepped internal pressure, a set of dynamic equations is set up using the membrane theory with a modal approach (bending moments are neglected with this theory). As already commonly established, it is found that radial and axial displacements are coupled, resulting in a Multi-Degree Of Freedom (MDOF) model with coupling. The maximum DLF of the cylinder is therefore determined for both radial and axial displacements. It is found that the axial DLF reaches a maximum value when there is a specific ratio between the radius and the length (parameter $\pi R/L$ equal to 1.0), while the radial DLF does not depend on the geometry.

Results are compared to Finite Elements dynamic simulations. On the whole, the dynamic results are validated for long cylinders (*i.e.* $\pi R/L \leq 0.1$). However, differences in the axial displacement tend to increase with an increase in the ratio R/L (shorter cylinders).

The regular value of 2.0 established for the Single Degree Of Freedom model and for both axial and radial directions is exceeded when the radial and axial modes are coupled. The difference can be significantly higher (DLF$\geq$ 3.9).

Keywords
Dynamic Load Factor, Elastic cylinders, Coupled Multi-Degree Of Freedom (MDOF) model, Internal pressure, Analytical model, Modal approach

1   Introduction

In the framework of nuclear severe accident analysis, the "Commissariat à l'Energie Atomique et aux Energies Alternatives" (CEA) considered the opportunity to build a new experimental facility [1-2]. It aims at analysing the reaction between corium and cooling fluid for Light Water Reactors (LWR) and Sodium Fast Reactors (SFR) on the one hand, and on studying relevant mitigation solutions on the other hand. These reactions produce pressure waves and involve materials or fluids that need to be contained in the facility. Vessels are used to guarantee this function, which means they must be designed with appropriate methods. Dynamic loads must be considered since the vessel response depends not only on the magnitude of the load, but also on its transient profile regarding the vessel characteristics (material, geometry). Such loads may lead to higher stress and deformation than those observed for the same loading applied statically, introducing the notion of Dynamic Load Factor (DLF). This expresses the ratio between dynamic displacement and static displaced, as defined in [3]. Usual design rules consider the value of 2.0 (see below for a justification in current situations) as a maximum DLF value, simplifying the processes related to dynamic effects with simple computation of static problems. However, this maximum value is proven wrong for the components of interest in the present research, yielding the need for more advanced analyses, in order to provide updated safe values of the DLF that can be used with static computation for the design of the considered vessels. It is reminded that such design rules are based on pure elastic computations, producing

---

[1] Corresponding author
E-mail address: christophe.garnier@cea.fr (C. Garnier)

maximum values to be compared to relevant criteria depending on the considered failure modes of the structures that can be analysed with the model set up. This latter point is an engineering post-processing step beyond the scope of the proposed research.

To this extent, the problem of cylindrical shells subjected to internal blast pressure has been extensively studied, either with analytical relations or with numerical techniques and for simple and complex loads [4-10]. One possible strategy is to establish and directly solve the dynamic equations of the cylinder taking into account the dynamic loading. A summary of the different dynamic equations is presented in [11] with multiple approaches. The simplest set of equations, namely the membrane theory, is based on membrane forces and disregards bending moments but considers thin cylinders. A set of dynamic equations are established and the modal behaviour is obtained as well as eigen-frequencies for torsional, radial, axial, circumferential and bending modes. It is shown that axial and radial displacements are related to each other (coupling effect) and interact.

However, the latter theory does not take into account the effect of the thickness, known to have an impact, especially on radial eigen-frequencies. It is commonly considered that the membrane theory fits relatively well for the previously identified modes of the cylinder in the case of a "long" geometry, $i.e.$ with a ratio between the length of the cylinder (L) and its radius (R) that is higher than unity and far from the extremities. In more general cases, bending moments must be added to membrane effects. For thin cylinders, such classical models can be cited: Donnell – Mushtari's equations [12-13], Love – Timoshenko's equations [14-15], and Flügge's equations [16]. Accurate equations of motion are also proposed in [11]. These models can be considered to explicitly solve the dynamic response of cylinders under the applied loading.

From a design viewpoint, however, only the maximum stress or strain response is relevant. Solving explicit equations does not always provide this information directly since the time of the maximum displacement cannot be predicted $a priori$ for all types of loading. This is especially the case for suddenly applied constant internal pressure (herein referred to as "stepped internal pressure" for convenience), which has an infinite duration. Only this type of loading function has been considered in this study. Using this specific loading is relevant and conservative in the proposed research since it generally produces maximum amplification factors when comparing static and dynamic maximum stress levels for the simplest model based on Single Degree of Freedom (SDOF) with damping ignored and for the usual loading functions described in Biggs [3]. Same methodology can be used for other shapes of time dependence loading.

A widely used engineering approach to design structures is based on the statements above and proposes to use the Dynamic Load Factor (DLF). For simple structures that can be modelled with the SDOF model, charts have been established for common simple loads [3]. These charts give the amplification needed to deduce the maximum elastic stress or strain in dynamic situations from equivalent and more affordable static computations. It is proven that the DLF has a maximum value of 2.0 for usual non-harmonic loads. This concept can be extended to simple Multiple-Degrees Of Freedom (MDOF) models and has been widely used to design beams and slabs for civil engineering applications [17-19], as well as spheres [20-21]. It has also been used to design cylinders using the SDOF model [22]. However, as previously mentioned, the coupling response between the radial and axial displacements for cylinders invalidates the SDOF or simple MDOF concepts. In this case, it is preferable to use an approach taking into account the relevant coupling and to determine the maximum value of the DLF. The obtained maximum value will be compared to the usual value of 2.0 for SDOF or simple MDOF models.

Biggs [3] once again describes an efficient tool for establishing the dynamic equations of structures and for computing the DLF, namely the Lagrange's equation. It can be applied in the case of multiple degrees of freedom: the structure is seen as an assembly of several SDOF models, each representing a natural mode. The equation is applied to each SDOF and the global response is computed as the sum of the responses of each mode. The DLF of each mode can be easily obtained and thus the global DLF as well. Some results are given for beams and slabs with the modal approach in [3]. In [23], the method is used to analyse the elastic pulse buckling of a thin cylindrical shell of finite length under cosine impulse. The equations take into account bending moments and only the first mode is considered.

The specific case of cylinders subjected to internal moving blast pressure and the associated DLF has also been largely studied [24-26]. The results of the above-mentioned references show that the maximum DLF can largely exceed the usual value obtained for SDOF, which once again invalidates this concept for the design of cylindrical structures.

Starting from the state-of-the-art report recalled above, this paper aims at providing a new and robust method to help improve engineering rules based on static computations. This method takes into account coupling between axial and radial modes and makes it possible to analytically determine maximum conservative values of the DLF

for elastic cylindrical structures in situations where the classical value of 2.0 no longer holds. The simple case of an open cylinder simply supported is considered (*i.e.* radial displacement is fixed at both extremities, whereas axial displacement and rotations are free), with no condition on its shape. It is subjected to stepped internal pressure. First, the dynamic response for both radial and axial displacements is obtained on basis of a modal analytical model using the membrane theory and the Lagrange's equation, resulting in a MDOF model with coupling. The maximum DLF values of the system for the axial and radial directions are conventionally deduced from the combination of the maximum DLF values computed for each modes. Conservative values (*i.e.* equal or higher than the maximum actual value) are finally established for design purposes. Contrary to solving explicit dynamic equations such as those presented in [11], this modal approach makes it possible to define analytical and conservative relations for the DLF. Relevance of the proposed approach is assessed through Finite Elements (FE) simulations of cylinders with various shapes (in term of ratio between radius and length).

This paper is organized as follows. In section 2, the dynamic equations of the cylinders integrating the coupling effect are first established with a modal approach. The conservative maximum values for DLF are then computed for each mode and are combined to obtain the resulting global DLF for the structure. In section 3, these results are compared to FE simulations, and the relevance and limits of the model are discussed.

2 DLF for cylinders based on a modal approach

2.1 Review of the DLF and global methodology

The Dynamic Load Factor, or DLF, is defined as follows, for a given location:

$$DLF(z) = \frac{\max|k(t)|}{|k_{st}|} \tag{1}$$

with $k(t)$ the displacement corresponding to time t, and k_{st} the static displacement, both obtained at the same given location. For convenience, $DLF(z)$ is noted DLF.

It can be computed for each point of the structure. The points of interest on cylinders are located at $z = L/2$ (mid-length) for radial displacement, and at $z = 0$ or $z = L$ (extremities) for axial displacement (see Fig. 1 for the reference coordinate system).

The followed approach sets out to establish dynamic equations to express cylinder movements, broken down into a series of modes to compute the maximum DLF for each mode, before finally determining the maximum value of DLF for the global response.

2.2 Dynamic modal equations for cylinders

[3] proposes a method to obtain the modal dynamic response of structures using Lagrange's equation. Based on energy concepts, it is a powerful tool for analysing dynamic systems. Biggs's approach is based on the principle of virtual work and is expressed as follows for the specific case of an undamped structure:

$$\frac{d}{dt}\left(\frac{\partial K}{\partial \dot{q}_i}\right) - \frac{\partial K}{\partial q_i} + \frac{\partial U}{\partial q_i} = \frac{\partial W}{\partial q_i} \tag{2}$$

with K, the kinetic energy, U, the strain energy, W, the work done by external forces, and q_i a set of generalized coordinates. It provides the equations of motion for each parameter q_i of the structure.

This equation can be applied to open cylinders subjected to stepped internal pressure $p(t)$. The membrane theory is used according to [11], *i.e.*: bending moments are not taken into account, the cylinder is considered as a thin object ($R/h > 10$) and shell deformations are small in comparison with the shell thickness. The boundary conditions correspond to a simply supported cylinder therefore the loads and boundary conditions are axisymmetric, and only axisymmetric modes are taken into account. The material is linear elastic and isotropic with following material parameters: ρ represents the density, E Young's modulus and ν Poisson's ratio. No damping effect is taken into account. Fig. 1 presents the cylindrical shell geometry with R representing the cylindrical tube mean radius, h the thickness and L the length. u, v, w are the displacement components at the mean radius location ($r = R$) along the z (axial), θ (transverse) and r (radial) axes respectively.
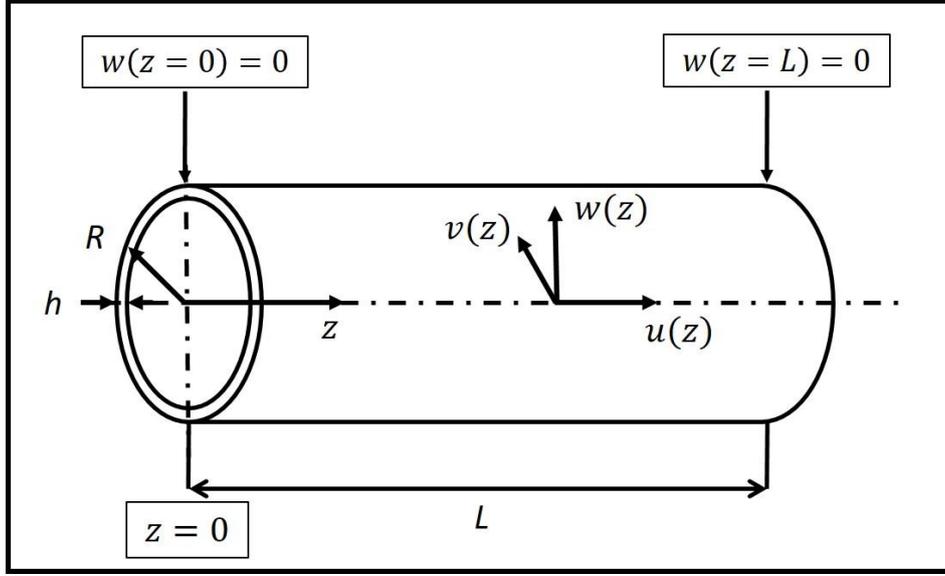
Fig. 1

Cylindrical shell geometry with simply supported extremities

The Lagrange equation is applied to a series of well-chosen modes of the cylinder, retrieving the complete displacement field when the mode index m tends towards the infinite. The displacement functions for each mode are taken from [11]:

$$\begin{aligned} u_m(z,t) &= C_{1m}(t) \cos \lambda_m^* z \\ v_m(z,t) &= 0 \\ w_m(z,t) &= C_{3m}(t) \sin \lambda_m^* z \end{aligned} \tag{3}$$

with $\lambda_m^* = \frac{m\pi}{L}$, m is an integer characterizing the mode ($m \geq 1$) and $C_{1m}(t), C_{3m}(t)$ are time dependant functions.

Only the odd modes are taken into account since the geometry and loading are symmetric with respect to the cylinder mid-length (u_m and w_m are symmetrical with respect to this plane). Therefore, m is expressed as: $m = 2n+1$ with n an integer ($n \geq 1$) and equations (3) become:

$$\begin{aligned} u_n(z,t) &= C_{1n}(t) \cos \lambda_n^* z \\ v_n(z,t) &= 0 \\ w_n(z,t) &= C_{3n}(t) \sin \lambda_n^* z \end{aligned} \tag{4}$$

w is positive for displacement moving from the inner to the outer radius of the cylinder.

The parameters q_i considered in (2) are C_{1n} and C_{3n}, which are representative of the radial and axial displacements for each mode. Therefore, the structure has 2 degrees of freedom per mode.

(2) can thus be applied to each mode n.

The kinetic energy K_n is [11]:

$$K_n = \frac{1}{2} \rho\, h \int_0^{2\pi} \int_0^L \left[\left(\frac{\partial u_n}{\partial t}\right)^2 + \left(\frac{\partial w_n}{\partial t}\right)^2 \right] R\, d\theta\, dz = \frac{1}{2} \pi \rho\, h\, R\, L \left(\dot{C}_{1n}^2 + \dot{C}_{3n}^2 \right)$$

$\frac{d}{dt}\left(\frac{\partial K_n}{\partial \dot{C}_{1n}}\right) = \pi \rho\, h\, R\, L\, \ddot{C}_{1n}, \frac{d}{dt}\left(\frac{\partial K_n}{\partial \dot{C}_{3n}}\right) = \pi \rho\, h\, R\, L\, \ddot{C}_{3n}.$

The strain energy U_n is [11]:

$$U_n = \frac{E\,h}{2\,(1-v^2)} \int_0^{2\pi} \int_0^L \left[\left(\frac{\partial u_n}{\partial z} - \frac{w_n}{R}\right)^2 + 2\,(1-v)\left(\frac{w_n}{R}\frac{\partial u_n}{\partial z}\right)\right] R\,d\theta\,dz$$

$$= \frac{\pi\,E\,h\,L\,R}{2\,(1-v^2)} \left(\lambda_n^{*\,2}\,C_{1n}^2 + \frac{C_{3n}^2}{R^2} + \frac{2\,v\,\lambda_n^*}{R}\,C_{1n}\,C_{3n}\right)$$

$$\frac{\partial U_n}{\partial C_{1n}} = \frac{\pi\,E\,h\,R\,L\,\lambda_n^*}{(1-v^2)}\left(\lambda_n^*\,C_{1n} + \frac{v}{R}\,C_{3n}\right), \frac{\partial U_n}{\partial C_{3n}} = \frac{\pi\,E\,h\,L}{(1-v^2)}\left(\frac{C_{3n}}{R} + v\,\lambda_n^*\,C_{1n}\right).$$

The work done by the external force (pressure) W_n is:

$$W_n = \int_0^{2\pi} \int_0^L p(t)\,w\,R\,d\theta\,dz = \frac{4\,\pi\,R\,p(t)}{\lambda_n^*}\,C_{3n}$$

$$\frac{\partial W_n}{\partial C_{1n}} = 0, \frac{\partial W_n}{\partial C_{3n}} = \frac{4\,\pi\,R\,p(t)}{\lambda_n^*}.$$

Finally, the following is true for each symmetric mode when using the mean radius of the cylinder:

$$\rho\,\ddot{C}_{1n} + \frac{E\,\lambda_n^{*\,2}}{(1-v^2)}\,C_{1n} = \frac{-E\,\lambda_n^*\,v}{(1-v^2)\,R}\,C_{3n}$$

$$\rho\,\ddot{C}_{3n} + \frac{E}{(1-v^2)\,R^2}\,C_{3n} = \frac{4\,p(t)}{\lambda_n^*\,L\,h} - \frac{E\,\lambda_n^*\,v}{(1-v^2)\,R}\,C_{1n}$$

(5)

The set of equations (5) is coupled, except for $v = 0$. It is a MDOF (2 degrees) model with coupling between the degrees of freedom in the general case and can be written in a matrix form.

By considering $X_n = \begin{bmatrix} C_{1n} \\ C_{3n} \end{bmatrix}$ and $\lambda_n = \lambda_n^*\,R = \frac{(2\,n+1)\,\pi\,R}{L}$, the set of equations (5) becomes:

$$\ddot{X}_n = \frac{-E}{(1-v^2)\,\rho\,R^2} \begin{bmatrix} \lambda_n^2 & \lambda_n\,v \\ \lambda_n\,v & 1 \end{bmatrix} X_n + \begin{bmatrix} 0 \\ \frac{4\,R\,p(t)}{\lambda_n\,\rho\,L\,h} \end{bmatrix} = A_n\,X_n + B_n$$

The principal directions of the system can be used to provide uncoupled equations in a new frame where:

$$\ddot{Y}_n = D_n\,Y_n + P^{-1}B_n$$

with P representing the transformation matrix such as: $A_n = P\,D_n\,P^{-1}$, D_n is a diagonal matrix,

and $Y_n = P^{-1}X_n = \begin{bmatrix} C_{1n} \\ C_{3n} \end{bmatrix}$.

P and D_n can be written as follows:

$$P = \frac{1}{2\,\lambda_n\,v} \begin{bmatrix} \lambda_n^2 - 1 - \sqrt{\varphi_n} & \lambda_n^2 - 1 + \sqrt{\varphi_n} \\ 2\,\lambda_n\,v & 2\,\lambda_n\,v \end{bmatrix}$$

$$D_n = \frac{-E}{2\,R^2\,\rho\,(1-v^2)} \begin{bmatrix} \lambda_n^2 + 1 - \sqrt{\varphi_n} & 0 \\ 0 & \lambda_n^2 + 1 + \sqrt{\varphi_n} \end{bmatrix}$$

(6)

with $\varphi_n = (\lambda_n^2 - 1)^2 + 4\,v^2\,\lambda_n^2$

In the new frame, a classical form of the SDOF dynamic equation is reached:

$$\ddot{c}_{1n} + \omega_{1n}^2 c_{1n} = F_{1n}$$

$$\ddot{c}_{3n} + \omega_{3n}^2 c_{3n} = F_{3n}$$

(7)

with ω_{1n}, ω_{3n} the natural pulsation for each symmetric mode either in a radial or axial direction:

$$\omega_{1n}^2 = \frac{E}{2 R^2 \rho (1 - v^2)} \left[\lambda_n^2 + 1 - \sqrt{\varphi_n}\right]$$

$$\omega_{3n}^2 = \frac{E}{2 R^2 \rho (1 - v^2)} \left[\lambda_n^2 + 1 + \sqrt{\varphi_n}\right]$$

(8)

$$\omega_{1n} \leq \omega_{3n}$$

The results for the natural pulsations of a cylinder as presented in [11] are retrieved. Correspondence between the two values of the natural pulsations and the type of mode (radial or axial) can be deduced from the relative rank of $|\Omega_{in}^2 - 1|$ with $\Omega_{in}^2 = \frac{\rho}{E}(1 - v^2) \omega_{in}^2 R^2$ ($i = \{1; 3\}$): the minimum value of $|\Omega_{in}^2 - 1|$ between its two values $|\Omega_{1n}^2 - 1|$ and $|\Omega_{3n}^2 - 1|$ corresponds to the radial mode. This set of equations (8) can be applied to both symmetric and anti-symmetric modes (m can take both odd and even values). However, only symmetric modes are relevant to this problem.

2.3 Computing the response of the system to a stepped internal pressure

The specific case of a stepped internal pressure is now considered. The applied load is shown in Fig. 2 and can be described as follows:

For $t \leq 0$: $p(t) = 0$

For $t \geq 0$: $p(t) = p_0$

For $t = 0$, $u(t = 0) = w(t = 0) = 0$ and $\dot{u}(t = 0) = \dot{w}(t = 0) = 0$.
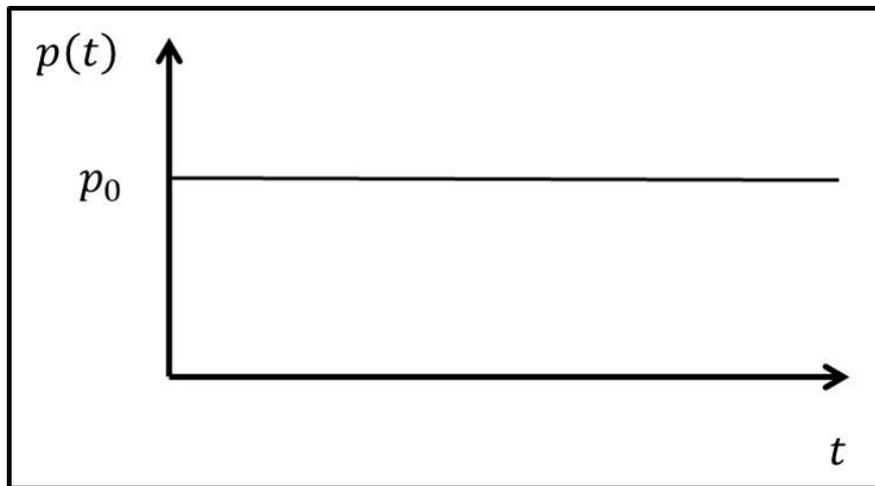

Fig. 2

Stepped internal pressure

The solutions of the uncoupled equations are classically given by:

$$\begin{bmatrix} c_{1n} \\ c_{3n} \end{bmatrix} = \begin{bmatrix} K_{1n} (1 - \cos \omega_{1n} t) \\ K_{3n} (1 - \cos \omega_{3n} t) \end{bmatrix}$$

with:

$$\begin{bmatrix} K_{1n} \\ K_{3n} \end{bmatrix} = \frac{2\,R\,p_0}{\rho\,L\,h}\,\frac{1}{\lambda_n\,\sqrt{\varphi_n}}\begin{bmatrix} \dfrac{\sqrt{\varphi_n} + \lambda_n^2 - 1}{\omega_{1n}^2} \\[2mm] \dfrac{\sqrt{\varphi_n} - (\lambda_n^2 - 1)}{\omega_{3n}^2} \end{bmatrix} \qquad (9)$$

The solutions of the coupled equations (5) can then be deduced:

$$X_n = \begin{bmatrix} C_{1n} \\ C_{3n} \end{bmatrix} = P\,Y_n = \begin{bmatrix} P_{11}\,K_{1n}\,(1 - \cos\omega_{1n}t) + P_{12}\,K_{3n}\,(1 - \cos\omega_{3n}t) \\ P_{21}\,K_{1n}\,(1 - \cos\omega_{1n}t) + P_{22}\,K_{3n}\,(1 - \cos\omega_{3n}t) \end{bmatrix} \qquad (10)$$

The displacement for each mode is equivalent to the sum of two oscillating terms with different pulsations. Their relative magnitude depends on the ratio of $\frac{P_{11}\,K_{1n}}{P_{12}\,K_{3n}}$ for C_{1n} and $\frac{P_{21}\,K_{1n}}{P_{22}\,K_{3n}}$ for C_{3n}.

Note that similar relations can be obtained for other classical loading functions $p(t)$.

The displacement response for each symmetric mode $2\,n + 1$ can be obtained from the set of equations (2) and (10). Finally, the global response of the cylinder is the sum of all modal contributions, *i.e.*:

$$u(z,t) = \sum_{n=0}^{\infty} u_n(z,t) \text{ and } w(z,t) = \sum_{n=0}^{\infty} w_n(z,t).$$

2.4 Computing static deformation

Static deformation can be obtained using a similar method without time dependency:

$$\begin{aligned} u_{st\,n}(z) &= C_{1n}\cos\lambda_n^* z \\ v_{st\,n}(z) &= 0 \\ w_{st\,n}(z) &= C_{3n}\sin\lambda_n^* z \end{aligned} \qquad (11)$$

with λ_n^* equal to the definition given for the set of equations (3).

The loading is constant and equal to p_0. From (5), it can be said that:

$$\begin{aligned} \lambda_n\,C_{1n} + \nu\,C_{3n} &= 0 \\ \frac{E}{(1 - \nu^2)\,R^2}\,(\lambda_n\,\nu\,C_{1n} + C_{3n}) &= \frac{4\,p_0\,R}{\lambda_n\,L\,h} \end{aligned} \qquad (12)$$

This can be simplified as follows:

$$A_n\,X_n = B_n$$

with $X_n = \begin{bmatrix} C_{1n} \\ C_{3n} \end{bmatrix}$, $A_n = \begin{bmatrix} \lambda_n & \nu \\ \lambda_n\,\nu & 1 \end{bmatrix}$ and $B_n = \begin{bmatrix} 0 \\ \frac{4\,p_0\,R^3\,(1-\nu^2)}{\lambda_n\,L\,h\,E} \end{bmatrix}$.

It can be easily solved:

$$\begin{bmatrix} C_{1n} \\ C_{3n} \end{bmatrix} = \frac{4\,p_0\,R}{(2\,n + 1)\,\pi\,E\,h}\begin{bmatrix} \dfrac{\nu\,L}{(2\,n + 1)\,\pi} \\ R \end{bmatrix}$$

The static displacements are equivalent to the sum of all the previous terms (C_{1n} and C_{3n}) combined with the spatial term from the set of relations (3).

$$u_{st}(z) = \sum_{n=0}^{\infty} u_{st\,n} = \frac{4\,p_0\,\nu\,R\,L}{\pi^2\,E\,h}\sum_{n=0}^{\infty}\frac{1}{(2\,n + 1)^2}\cos\frac{(2\,n + 1)\,\pi\,z}{L} \qquad (13)$$

$$w_{st}(z) = \sum_{n=0}^{\infty} w_{st\,n} = \frac{4\,p_0\,R^2}{\pi\,E\,h} \sum_{n=0}^{\infty} \frac{1}{2\,n+1} \sin\frac{(2\,n+1)\,\pi\,z}{L} \qquad (14)$$

With regard to axial displacement (equation (13)):

For $z = 0$ and $z = L$, $\cos\frac{(2\,n+1)\,\pi\,z}{L} = \pm 1$, and $\sum_{n=0}^{\infty} \frac{1}{(2\,n+1)^2} = \frac{\pi^2}{8}$

$$u_{st}(z = 0) = -u_{st}(z = L) = \frac{\nu\,p_0\,R\,L}{2\,E\,h} \qquad (15)$$

With regard to radial displacement (equation (14)):

$\sum_{n=0}^{\infty} \frac{1}{2\,n+1} \sin\frac{(2\,n+1)\,\pi\,z}{L} = \frac{\pi}{4}$ for $0 \leq z \leq L$.

Therefore, for $z = L/2$:

$$w_{st}(z = L/2) = \frac{p_0\,R^2}{E\,h} \qquad (16)$$

These results are consistent with the formulas given in [29] for infinite thin cylinders subjected to internal pressure. Because of the membrane theory, the results for finite cylinders are equivalent to infinite geometry except for extremities. These relations can be used to compute the DLF.

2.5 Computing the DLF for each mode

The set of equations (10) is used to compute the maximum value of the DLF for the stepped pressure loading and for each mode.

In the following, the shape of the cylinder (mean radius R and length L) is defined with the parameter $\lambda_0 = \lambda_n(n = 0) = \frac{\pi\,R}{L}$. Therefore, any value of λ_n can be expressed using this parameter: $\lambda_n = (2\,n+1)\,\lambda_0$.

2.5.1 Radial displacement

With regard to radial displacement and based on (10), C_{3n} can be expressed as:

$$C_{3n} = P_{21}\,K_{1n}\,(1 - \cos\omega_{1n}\,t) + P_{22}\,K_{3n}\,(1 - \cos\omega_{3n}\,t)$$

$$0 \leq 1 - \cos\omega_{in}\,t \leq 2 \ (i = \{1;\,3\})$$

$P_{21}\,K_{1n}$ and $P_{22}\,K_{3n}$ can be computed from equations (6) and (9).

Since $\sqrt{\varphi_n} \geq \lambda_n^2 - 1$, K_{3n} is always positive and so is $P_{22}\,K_{3n}$ as P_{22} is equal to 1.

It can also be shown that $\sqrt{\varphi_n} + \lambda_n^2 - 1$ is always positive for $\lambda_n \geq 0$, therefore K_{1n} is always positive and so is $P_{21}\,K_{1n}$ since P_{21} is equal to 1.

Finally, overestimation of this sum of cosine terms is classically obtained by summing the maximum value of each term.

Thus:

$$0 \leq C_{3n} \leq 2 \left(P_{21} K_{1n} + P_{22} K_{3n}\right) = \frac{8 R^2 p_0}{\pi E h} \frac{1}{(2 n + 1)}$$

The radial displacement can be obtained with equation (3). The DLF can therefore be evaluated for $z = L/2$. It therefore results that:

$$w_n \left(z = \frac{L}{2}\right) = C_{3n} \sin \frac{(2 n + 1) \pi}{2} = (-1)^n C_{3n}$$

For even values of n ($n \to 2\,k$): $0 \leq w_{4\,k+1}(z = \frac{L}{2}) \leq \frac{8 R^2 p_0}{\pi E h} \frac{1}{4\,k+1}$

For odd values of n ($n \to 2\,k+1$): $\frac{-8 R^2 p_0}{\pi E h} \frac{1}{4\,k+3} \leq w_{4\,k+3} \left(z = \frac{L}{2}\right) \leq 0$ $\qquad$ (17)

As the DLF is computed with the absolute values, the following is true whatever the value of n:

$$\left| w_n \left(z = \frac{L}{2}\right) \right| \leq \frac{8 R^2 p_0}{\pi E h} \frac{1}{(2 n + 1)}$$

Based on equation (16), the maximum value of the DLF (based on the absolute value of displacement) in the radial direction for each symmetric mode and for $z = L/2$ is:

$$DLF_n \left(w \left(z = \frac{L}{2}\right)\right) = \frac{|w_n|}{|w_{st}|} \leq \frac{8}{(2 n + 1) \pi} \qquad (18)$$

It is observed *a posteriori* that this DLF does not depend on the geometry of the cylinder and especially on the ratio R/L. It only depends on the considered symmetric mode. Such results are observed for SDOF model with same loading function (Biggs [3]).

2.5.2 Axial displacement

With regard to the axial direction and from (10), C_{1n} can be expressed as:

$$C_{1n} = P_{11} K_{1n} \left(1 - \cos \omega_{1n} t\right) + P_{12} K_{3n} \left(1 - \cos \omega_{3n} t\right)$$

From (6) and (9): $P_{11} K_{1n} = -\frac{4 R P_0 \nu}{\rho L h} \frac{1}{\sqrt{\varphi_n} \omega_{1n}^2}$ and $P_{12} K_{3n} = \frac{4 R P_0 \nu}{\rho L h} \frac{1}{\sqrt{\varphi_n} \omega_{3n}^2}$.

An overestimation of this sum of cosine terms is classically obtained by summing the maximum value of each term.

Thus, it results that:

$$C_{1n} = \frac{4 R P_0 \nu}{\rho L h} \frac{1}{\sqrt{\varphi_n}} \left(\frac{1 - \cos \omega_{3n} t}{\omega_{3n}^2} - \frac{1 - \cos \omega_{1n} t}{\omega_{1n}^2}\right) \qquad (19)$$

Since $\omega_{3n} \geq \omega_{1n}$, the maximum absolute value of (19) is given by:

$$|C_{1n}| \leq \frac{4 R P_0 \nu}{\rho L h} \frac{1}{\sqrt{\varphi_n}} \left| \frac{0}{\omega_{3n}^2} - \frac{2}{\omega_{1n}^2} \right| = \frac{16 \nu (1 - \nu^2) R^3 p_0}{E L h} \frac{1}{\sqrt{\varphi_n} \left(\lambda_n^2 + 1 - \sqrt{\varphi_n}\right)}$$

The axial displacement can be expressed with equation (3). For $z = 0$ and $z = L$:

$$u_n(z = 0, t) = C_{1n}(t) = -u_n(z = L, t)$$

Thus:

$$|u_n(z = 0)| = |u_n(z = L)| \leq \frac{16 \, v \, (1 - v^2) \, R^3 \, p_0}{E \, L \, h} \frac{1}{\sqrt{\varphi_n} \, (\lambda_n^2 + 1 - \sqrt{\varphi_n})}$$

With (15), $DLF_n(u)$ can be expressed for $z = 0$ or $z = L$ (highest axial static displacement):

$$DLF_n(u(z = 0)) = DLF_n(u(z = L)) = \frac{Max(|u_n|)}{|u_{st}|} \leq \frac{32 \, (1 - v^2)}{(2 \, n + 1)^2 \, \pi^2} \frac{\lambda_n^2}{\sqrt{\varphi_n} \, (\lambda_n^2 + 1 - \sqrt{\varphi_n})} \qquad (20)$$

Unlike radial displacement, the axial DLF this time depends on both the geometry (ratio R/L through the parameter λ_n) and Poisson's ratio, which can be attributed to the more complex nature of the axial displacement induced by internal radial pressure loading.

The function $f(\lambda_n) = \frac{\lambda_n^2}{\sqrt{\varphi_n} \, (\lambda_n^2 + 1 - \sqrt{\varphi_n})}$ presents a maximum value for $\lambda_n = \lambda_c = 1 \, \forall \, n$. This value is equal to $f(\lambda_n = 1) = \frac{1}{4 \, v \, (1 - v)}$. Therefore, the maximum possible value of $DLF_n(u)$ is reached for $\lambda_c \, \forall \, n$, with $Max(DLF_n(u)) = \frac{8}{(2 \, n + 1)^2 \, \pi^2} \frac{1 + v}{v}$.

This maximum value corresponds to the switch between the two modes, *i.e.* the radial and axial modes: for $\lambda_n < 1$, ω_{1n} corresponds to the axial mode whereas ω_{3n} represents the radial mode. Modes are inverted for $\lambda_n > 1$.

2.5.3 Evolution of the DLF in both directions with respect to the shape of the cylinder

Fig. 3 presents the variations in the DLF with respect to λ_0 ($\lambda_0 \neq 0$) for both directions and for the first symmetric mode (*i.e.* $n = 0$): $DLF_{n=0}(u)$ represents the DLF for the axial direction whereas $DLF_{n=0}(w)$ represents the radial direction. v is considered equal to 0.33. The dashed curves represent the specific values of $DLF = 1.0$ (red curve) and $DLF = 2.0$ (green curve). First, $DLF_{n=0}(u) > DLF_{n=0}(w)$ in the case of some values for λ_0. Moreover, both DLF are always greater than 1.0 (red curve), which means that the displacement is always amplified. Therefore, $DLF_{n=0}(w)$ is always higher than 2.0 (green curve), whereas $DLF_{n=0}(u)$ only exceeds this specific value in the case of some values for λ_0 (around λ_0=1). This means that the usual value for the SDOF model ($DLF = 2.0$) can be exceeded in both directions.
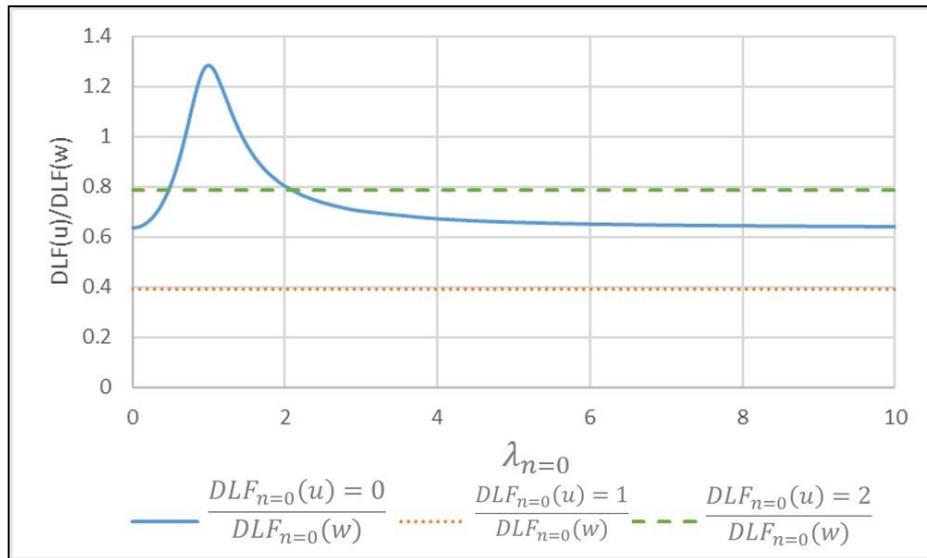

Fig. 3

$DLF_{n=0}(u)$ and $DLF_{n=0}(w)$ with respect to λ_0 for the first symmetric mode ($n = 0$) and v=0.33

2.6 Estimating the global DLF taking into account all the modes

In this section, an estimation of the value of the DLF is presented for each direction taking into account all modes.

The global response of the cylinder is equivalent to the sum of all the modes. Therefore, for each position z, the DLF can be expressed as:

$$DLF(u) = \frac{max|\sum_{n=0}^{\infty} u_n(z,t)|}{|\sum_{n=0}^{\infty} u_{st_n}(z)|} = \frac{max|\sum_{n=0}^{\infty} C_{1n}(t) \cos \lambda_n^* z|}{|\sum_{n=0}^{\infty} C_{1n} \cos \lambda_n^* z|}$$

$$DLF(w) = \frac{max|\sum_{n=0}^{\infty} w_n(z,t)|}{|\sum_{n=0}^{\infty} w_{st_n}(z)|} = \frac{max|\sum_{n=0}^{\infty} C_{3n}(t) \sin \lambda_n^* z|}{|\sum_{n=0}^{\infty} C_{3n} \sin \lambda_n^* z|}$$

(21)

The maximum value of both DLF can be found with respect to the position z. However, in this paper, only the following cases are considered: $z = L/2$ for the radial direction, and $z = 0$ or $z = L$ for the axial direction.

Therefore, the set of equations (21) becomes:

$$DLF\big(u(z = 0)\big) = \frac{max|\sum_{n=0}^{\infty} C_{1n}(t)|}{|\sum_{n=0}^{\infty} C_{1n}|}$$

$$DLF\big(w(z = L/2)\big) = \frac{max|\sum_{n=0}^{\infty} C_{3n}(t)|}{|\sum_{n=0}^{\infty} C_{3n}|}$$

(22)

Previous expressions used to compute the DLF of each mode for $C_{1n}(t)$ and $C_{3n}(t)$ can be employed to estimate the global resulting DLF. It should be remembered that some conservative assumptions have been applied to obtain these relations. It appears that the axial DLF depends on λ_n (which depends on the cylinder shape with $\lambda_n = (2n + 1)\lambda_0$.

Several methods can be used to compute the global DLF.

The most conservative method involves directly summing all the previously computed DLF values for each mode. It is noted as DLF_{sum}. This implies that all the oscillating terms reach their maximum value at the same time so they can be summed together. For each direction:

$$DLF_{sum}(u,w) = \sum_{n=0}^{\infty} DLF_n(u,w)$$

(23)

Another approach involves using the Root Mean Square (RMS) relation based on the DLF for each mode:

$$DLF_{RMS}(u,w) = \sqrt{\sum_{n=0}^{\infty} \big(DLF_n(u,w)\big)^2}$$

(24)

The conservatism of this relation cannot be guaranteed *a priori*. This point is analysed in section 3 of the paper.

These two relations can be applied for both directions, axial and radial directions.

The global DLF for the radial direction is computed at $z = L/2$ and is designated as $DLF_{sum}(w)$ or $DLF_{RMS}(w)$ depending on the method used to compute it. The global DLF for the axial direction is computed at $z = 0$ and $z = L$. As the response proved to be symmetric, it has the same value for both locations. It is noted as $DLF_{sum}(u)$ or $DLF_{RMS}(u)$ depending on the method used to compute it.

2.6.1 Radial displacement

With regard to the radial direction, the set of equations (17) can be used for each mode. Instead of considering the absolute value for one single mode, the sign of each term must be taken into account when contributing to the sum.

However, in order to maximize the value of the global DLF, the following considerations must be taken into account:

- For even values of n ($n \rightarrow 2\,k$): $0 \leq w_n(z = \frac{L}{2}) \leq \frac{8\,R^2\,p_0}{\pi\,E\,h}\,\frac{1}{4\,k+1}$
- For odd values of n ($n \rightarrow 2\,k+1$): $w_n\left(z = \frac{L}{2}\right) \leq 0$
- The displacement tends to be outwards. Therefore, the maximum displacement should be positive.

Thus, only even values of n are taken into account, corresponding to $m = 4\,k + 1$ with k integer and $k \geq 0$. In order to obtain homogenous notations, k is replaced with n (n integer and $n \geq 0$). **This is a very conservative assumption.** With (16), it results in:

$$DLF_{sum}(w) = \frac{8}{\pi} \sum_{n=0}^{\infty} \frac{1}{(4\,n+1)} \tag{25}$$

This series diverges and no overestimate can be defined. However, a truncation of this series can provide an overestimate. The number of modes to be taken into account can be obtained from the convergence analysis needed to select the main modes contributing to the dynamic response described in section 3.

The series containing all the terms (either negative or positive) converges, which means the DLF can be expressed as follows:

$$\frac{8}{\pi} \sum_{n=0}^{\infty} \frac{(-1)^n}{(4\,n+1)} = 2.0 \leq DLF_{sum}(w)$$

This result shows that the classical DLF value for the SDOF model is exceeded for the cylinder.

With the RMS method:

$$DLF_{RMS}(w) = \frac{8}{\pi} \sqrt{\sum_{n=0}^{\infty} \frac{1}{(4\,n+1)^2}} \tag{26}$$

The results are not precisely known. However, it is worth noting the following relations:

$$1 \leq \sum_{n=0}^{\infty} \frac{1}{(4\,n+1)^2} \leq \sum_{n=0}^{\infty} \frac{1}{(2\,n+1)^2} = \frac{\pi^2}{8}$$

$$\frac{8}{\pi} \leq DLF_{RMS}(w) \leq \frac{4}{\sqrt{2}}$$

This result is still higher than 2.0.

The previous results are summarised in table 2.

$DLF_{sum}(w)$	$2.0 \leq DLF_{sum}(w) \leq \frac{8}{\pi} \sum_{k=0}^{n} \frac{1}{(4\,k+1)}$ (truncation up to mode n)
$DLF_{RMS}(w)$	$\frac{8}{\pi} \leq DLF_{RMS}(w) \leq \frac{4}{\sqrt{2}}$

Table 1: Synthesis of the different methods and approximations used to compute the global radial DLF

2.6.2 Axial displacement

With regard to the axial direction, the sum method results in the following for $z = 0$ or $z = L$ and from equation (20):

$$DLF_{sum}(u) = \frac{32\,(1-\nu^2)}{\pi^2} \sum_{n=0}^{\infty} \frac{1}{(2\,n+1)^2} \frac{\lambda_n{}^2}{\sqrt{\varphi_n}\,(\lambda_n^2 + 1 - \sqrt{\varphi_n})} \qquad (27)$$

The result of this series is not known. However, an upper bound can be found by considering that the maximum value of $\frac{\lambda_n{}^2}{\sqrt{\varphi_n}\,(\lambda_n^2 + 1 - \sqrt{\varphi_n})}$ is obtained for $\lambda_n = \lambda_c = 1$. It should be remembered that λ_n depends on n. This quantity is first maximized for the first symmetric mode, i.e. m=1 or n=0: $\lambda_0 = 1$. Therefore:

$$\lambda_n = m\,\lambda_0 = m = (2\,n+1)\ \forall\ n$$

The associated DLF ($DLF_{sum}(u, \lambda_n = (2\,n+1))$) can be expressed as follows:

$$DLF_{sum}(u) \le DLF_{sum}(u, \lambda_n = (2\,n+1)) = \frac{32\,(1-\nu^2)}{\pi^2} \sum_{n=0}^{\infty} \frac{1}{\sqrt{\varphi_n}\,((2\,n+1)^2 + 1 - \sqrt{\varphi_n})} \qquad (28)$$

with φ_n expressed as: $\varphi_n = ((2\,n+1)^2 - 1)^2 + 4\,\nu^2\,(2\,n+1)^2$.

This expression no longer depends on λ_n and consequently can be applied to any cylinder. However, the exact result is unknown and has to be approximated by means of truncation. This point is discussed in part 3. Nevertheless, the series is always higher than its first term (i.e. n=0):

$$\frac{8\,(1+\nu)}{\pi^2\,\nu} \le DLF_{sum}(u, \lambda_n = (2\,n+1))$$

The minimum value can be obtained for $\nu = 0.5$: $DLF_{sum}(u, \lambda_n = (2\,n+1)) \ge \frac{24}{\pi^2}$. This result is higher than the usual value of 2.0 for the SDOF model.

A further conservative simplification can be applied, i.e. $\lambda_n = \lambda_c = 1$ whatever the value considered for n. The following simplifications therefore apply:

$\frac{32\,(1-\nu^2)\,\lambda_n{}^2}{\pi^2\,\sqrt{\varphi_n}\,(\lambda_n^2 + 1 - \sqrt{\varphi_n})} = \frac{8\,(1+\nu)}{\pi^2\,\nu}$ and $\sum_{n=0}^{\infty} \frac{1}{(2\,n+1)^2} = \frac{\pi^2}{8}$.

The associated DLF ($DLF_{sum}(u, \lambda_n = 1)$) is then:

$$DLF_{sum}(u) \le DLF_{sum}(u, \lambda_n = 1) = \frac{(1+\nu)}{\nu} \qquad (29)$$

In this case, the exact result can be computed, though more conservative.

In order to illustrate the previous results, an example is provided here below. The axial DLF is computed with the first three symmetric modes ($m = 2\,n+1 \le 5$) and by using the three previous methods. The value of $\lambda_0 = 0.5$ is considered. Fig. 4 illustrates the different intermediate and final results. The basic method uses the full expression of the DLF ($DLF_{sum}(u)$ with (27)). For $\lambda_0 = 0.5$, the DLF values for the first three symmetric modes correspond to markers 1, 2 and 3. The value 4 is the sum of the three previous terms. The second method ($DLF_{sum}(u, \lambda_n = (2\,n+1))$ with relation (28)), which is more conservative, does not take into account the actual value of lambda, but sets it at $\lambda_0 = 1$. The results for the three considered modes correspond to markers 5, 6 and 7. The resulting DLF is associated with marker 8. Finally, the last method is the most conservative ($DLF_{sum}(u, \lambda_n = 1)$ with relation (29)): it considers that λ_n is equal to 1.0 for all modes (all odd values of m). The associated markers are referenced 9, 10 and 7. The resulting sum corresponds to marker and line 11. The relative rank between the methods (reflecting their conservatism) is highlighted with this simple example.
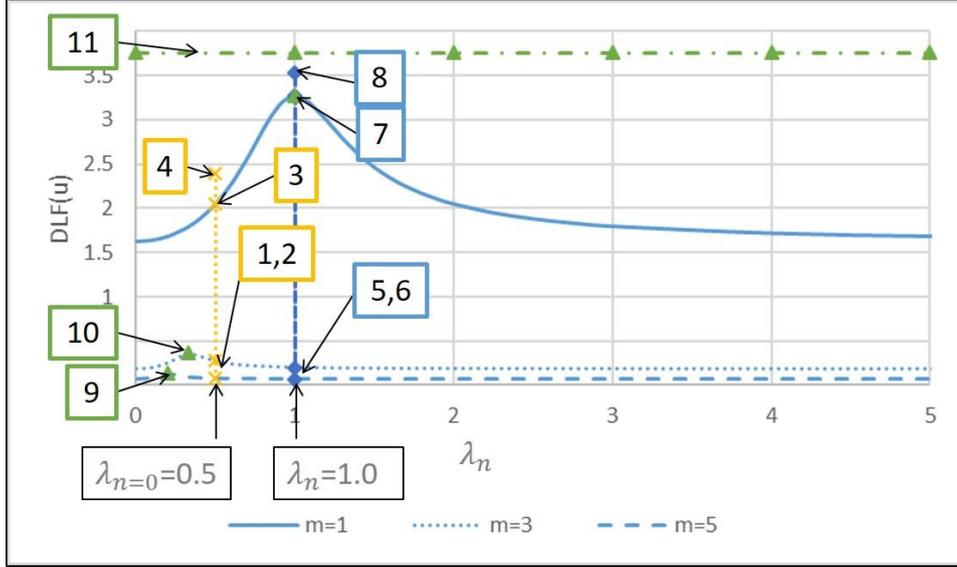
Fig. 4

Computing the axial DLF using the different methods for $\lambda_0 = 0.5$ and for $v = 0.33$

With the RMS method and for $z = 0$ or $z = L$:

$$DLF_{RMS}(u) = \sqrt{\sum_{n=0}^{\infty} \left(DLF_n(u)\right)^2} \qquad (30)$$

As previously explained for the sum method, this quantity can be maximized by first considering λ_0 equal to 1.

$$DLF_{RMS}(u, \lambda_n = (2\,n+1)) = \frac{32\,(1-v^2)}{\pi^2} \sqrt{\sum_{n=0}^{\infty} \left(\frac{1}{\sqrt{\varphi_n}\left((2\,n+1)^2 + 1 - \sqrt{\varphi_n}\right)}\right)^2} \qquad (31)$$

with φ_n expressed as: $\varphi_n = ((2\,n+1)^2 - 1)^2 + 4\,v^2\,(2\,n+1)^2$.

$$DLF_{RMS}(u) \leq DLF_{RMS}(u, \lambda_n = (2\,n+1))$$

This expression no longer depends on λ_n and can be applied to any cylinder. However, the exact result is not known and has to be approximated with truncation. Nevertheless, just like the sum method, the series is always higher than its first term (*i.e.* n=0):

$$\frac{8\,(1+v)}{\pi^2\,v} \leq DLF_{RMS}(u, \lambda_n = (2\,n+1))$$

Like the sum method, $DLF_{RMS}(u, \lambda_n = (2\,n+1)) \geq \frac{24}{\pi^2}$. This result is higher than the usual value of 2.0 for the SDOF model.

Again like the sum method, a further conservative simplification can be considered, *i.e.* that $\lambda_n = \lambda_c = 1$ whatever the value for n. Therefore, the following simplification can be applied:

$$DLF_{RMS}(u, \lambda_n = 1) = \frac{8\,(1+\nu)}{\pi^2\,\nu}\sqrt{\sum_{n=0}^{\infty}\frac{1}{(2\,n+1)^4}}$$

And given that:

$$\sum_{n=0}^{\infty}\frac{1}{(2\,n+1)^4} = \frac{\pi^4}{96}$$

$$DLF_{RMS}(u, \lambda_n = 1) = \frac{2}{\sqrt{6}}\frac{(1+\nu)}{\nu} = \frac{2}{\sqrt{6}}\,DLF_{RMS}(u, \lambda_n = 2\,n+1)$$

(32)

and:

$$DLF_{RMS}(u) = \sqrt{\sum_{n=0}^{\infty}\big(DLF_n(u)\big)^2} \le DLF_{RMS}(u, \lambda_n = 1)$$

The previous results are summarised in table 2.

	Full expression	First conservative approximation $\lambda_0 = 1$	Second conservative approximation $\lambda_n = 1\ \forall\ n$
$DLF_{sum}(u)$	Equation (27) $DLF_{sum}(u)$ Truncation needed	Equation (28) $DLF_{sum}\big(u, \lambda_n = (2\,n+1)\big)$ Truncation needed $\ge \dfrac{24}{\pi^2}$	Equation (29) $DLF_{sum}(u, \lambda_n = 1)$ $= \dfrac{(1+\nu)}{\nu}$
$DLF_{RMS}(u)$	Equation (30) $DLF_{RMS}(u)$ Truncation needed	Equation (31) $DLF_{RMS}(u, \lambda_n = (2\,n+1))$ Truncation needed $\ge \dfrac{24}{\pi^2}$	Equation (32) $DLF_{RMS}(u, \lambda_n = 1)$ $= \dfrac{2}{\sqrt{6}}\dfrac{(1+\nu)}{\nu}$ $= \dfrac{2}{\sqrt{6}}\,DLF_{sum}(u, \lambda_n = 1)$

Table 2: Summary of the different methods and approximations used to compute the global axial DLF

3 Assessment of the model and discussion

In this section, the above analytical results are compared with FE simulations.

The case in question consists of an open cylindrical test section. The loading and boundary conditions are identical to the configuration described in section 2, with an internal pressure of 30.6 MPa. The test section is made of aluminium. Table 3 specifies the parameters applied to the cylinder.

Density (ρ)	2685 kg/m^3
Young's modulus (E)	72300 MPa
Poisson's ratio (ν)	0.33
Mean radius (R)	0.1 m
Thickness (h)	0.007 m

Table 3: Parameters of the test section

The previously defined radius, R, is considered to be equal to the mean radius for the FE model.

The ratio R/h corresponds to a thin cylinder. The cylinder length L can be deduced from the applied value for λ_0. The following four cases are considered: $\lambda_0 = 0.1$, $\lambda_0 = 0.5$, $\lambda_0 = 1.0$ and $\lambda_0 = 2.0$. For $\lambda_0 < 1.0$, the cylinder is considered as long cylinder.

In the following sub-sections, the numerical tools used are first presented, *i.e.* the FE method and Discrete Fourier Transform (DFT). Then, both the FE and analytical models are compared on basis of the static displacement, the modal frequencies and the dynamic response. A preliminary analysis of the dynamic displacement is then provided to determine the number of modes to be integrated into the calculation (truncation of the modes). Finally, the DLF are determined for each cylinder so the effect of the parameter λ_0 can also be analysed.

As mentioned above, the locations relevant to the problem are the extremities ($z = 0$, $z = L$), and the mid-length of the cylinder ($z = L/2$).

3.1   Numerical methods

Two numerical tools are used: the FE Method (FEM) and a discrete formulation of Fast Fourier Transform (FFT), namely Discrete Fourier Transform (DFT).

A FE model is established to validate the previous dynamic analytical model. It is an axisymmetric transient model with simply supported extremities ($w(t, z = 0) = w(t, z = L) = 0$). As the geometry and the loading are symmetric with respect to the mid-plane at $z = L/2$, only a half-length is taken into account with symmetric conditions ($u(t, z = L/2) = 0$).

Regular quadrangles are used for meshing. The mesh is fine enough to capture all the main modes contributing to the dynamic response. Radial displacement is fixed at $z = 0$ for the node located on mean radius (mid-thickness of the wall). Internal pressure is applied to the inner radius. Fig. 5 illustrates the model in question. Cast3M [27] is used for simulations.
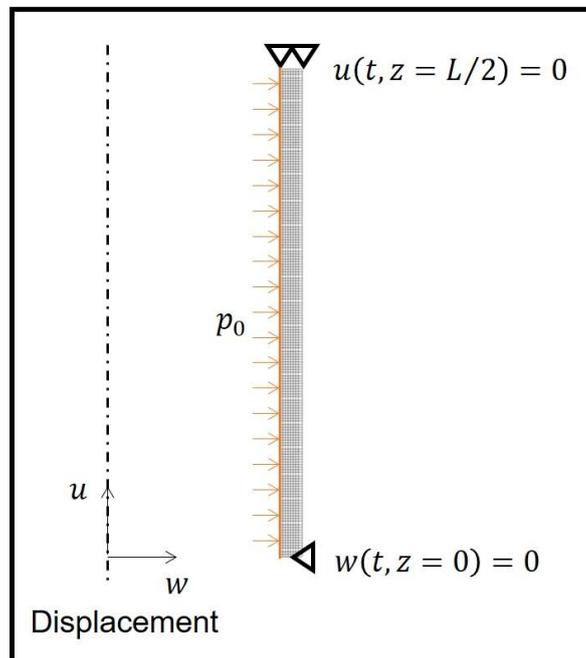

Fig. 5

FE transient axisymmetric model (half model with symmetrical condition)

As a preliminary step, it is worth completing a modal analysis to compute the eigen-modes and frequencies, and to compare the results with the previous analytical frequencies (given on basis of the parameters $\omega_{1,n}$ and $\omega_{3,n}$)

given by the set of relations (8). The previous half model only provides symmetric modes, which are the only modes participating in the dynamic response for this type of loading.

Therefore, the dynamic response can be obtained thanks to a transient analysis. The time step Δt is taken low enough to capture all the main modes contributing to the dynamic response. Its value is determined on basis of a classical convergence analysis of the dynamic results. The modes taken into account are progressively increased until the results stabilise.

The nodal displacements are post-processed at their previously defined locations ($z = 0$ and $z = L/2$) so they can be compared against the previously defined locations.

An equivalent model is used in a static configuration in order to compute the DLF. The results for the previous quantities are retrieved.

The second tool used is the discrete formulation of FFT. FFT is a very powerful tool for analysing the dynamic response of a structure. Its discrete formulation (Discrete Fourier Transformation, DFT) implemented in the Python code [28] is used (1-D discrete Fourier Transforms, see scipy.org). It can be used to obtain the natural frequencies of the modes contained in the dynamic response and to compare the different models (i.e. FE and analytical models). However, the quality of results depends on both the quantity of data and the time step. As previously explained, the maximum time step (or sampling frequency) depends on the maximum frequency of the modes involved in the response. Its value should not be too high in order to include the main modes. The other coupled parameter is the duration of the simulated response. The DFT frequency spacing (Δf) depends on both these parameters. The longer the duration is, the lower the frequency spacing (Δf). The objective value for Δf is fixed around 60 Hz, which requires an acceptable amount of samples. Therefore, the frequency values retrieved by the DFT (f) should be interpreted taking into account this interval: the actual frequency can be limited between $f - \Delta f/2$ and $f + \Delta f/2$.

3.2   Static response

The static displacements must be calculated in order to evaluate the DLF. In this part, they are calculated using the analytical relations given in section 2.4 and then compared to the results obtained with the FE model (static model).

Table 4 presents the results for both the analytical and FE models. Relative differences are low for radial displacement. The axial displacement is relatively low for the lowest value of λ_0 and increases with this parameter. The results for the axial displacement with the membrane theory are less accurate for short cylinders. Bending moments should be taken into account. Moreover, it should be remembered that the internal pressure is applied on the inner radius for the FE model, whereas it is applied on the mean radius for the analytical model. Consequently, the resulting difference is higher for thick cylinders, which is the case for the considered cylinders when λ_0 increases.

			λ_0			
			0.1	0.5	1.0	2.0
w_{st}	Analytical	mm	0.605	0.605	0.605	0.605
	FE	mm	0.590	0.590	0.590	0.610
	Relative difference	%	2.5	2.5	2.6	-0.9
u_{st}	Analytical	mm	3.13	0.627	0.273	0.157
	FE	mm	2.90	0.565	0.313	0.127
	Relative difference	%	8.1	11.0	14.8	23.4

Table 4: Static displacements

3.3   Modal analysis

Even if this paper does not set out to determine the validity of the results of the modal analysis using the membrane theory, frequency values have an impact on the dynamic results and are used to define the time step. Therefore, these results should be analysed in a first step.

Tables 5 and 6 present the natural frequencies for the axial and radial modes respectively. Here, both the symmetric and anti-symmetric modes are computed. The relative difference is calculated using the FE results as the reference: $\frac{(f_{analytical} - f_{FE})}{f_{FE}}$ (%). Even if a larger number of modes are used in the dynamic response, only the first main modes are presented.

The axial modes are practically identical between the two models. With regard to the radial modes, no significant difference can be observed for the lowest value of $\lambda_{n=0}$ ($\lambda_{n=0} = 0.1$). When $\lambda_{n=0}$ increases, differences can be observed for the modes higher than the first mode, as shown in Fig. 6. The difference increases with λ and with the mode number m (harmonics). However, the value for the first natural mode tends to be very close to the reference (FE value). These observations highlight the accuracy of the membrane theory for radial modes as long as the cylinder is long; this is true except for the first mode for which the results correlate well for any cylinder shape.

This analysis is supplemented with the DFT applied to the dynamic response.

λ_0		Unit	Axial mode		
			m		
			1	3	5
0.1	Analytical results	Hz	825	2465	4060
	FE results	Hz	825	2465	4060
	Relative difference	%	0.00	0.00	0.00
0.5	Analytical results	Hz	4060	13617	22093
	FE results	Hz	4060	13617	22087
	Relative difference	%	0.00	0.00	0.02
1.0	Analytical results	Hz	10090	26422	43843
	FE results	Hz	10090	26413	43793
	Relative difference	%	0.00	0.03	0.12
2.0	Analytical results	Hz	17799	52575	87537
	FE results	Hz	17797	52492	87103
	Relative difference	%	0.01	0.16	0.50

Table 5: Frequencies for axial modes – comparison between analytical results and FE results

λ_0		Unit	Radial mode			
			m			
			1	3	5	7
0.1	Analytical results	Hz	8754	8795	8899	9130
	FE results	Hz	8759	8800	8904	9134
	Relative difference	%	-0.06	-0.06	-0.05	-0.05
0.5	Analytical results	Hz	8899	7960	8176	8220
	FE results	Hz	8904	7965	8233	8460
	Relative difference	%	-0.05	-0.07	-0.69	-2.84
1.0	Analytical results	Hz	7161	8204	8240	8249
	FE results	Hz	7162	8329	9245	11631
	Relative difference	%	-0.01	-1.50	-10.9	-29.1
2.0	Analytical results	Hz	8119	8246	8254	8256
	FE results	Hz	8140	10224	18207	31060
	Relative difference	%	-0.26	-19.3	-54.7	-73.4

Table 6: Frequencies for radial modes – comparison between analytical results and FE results
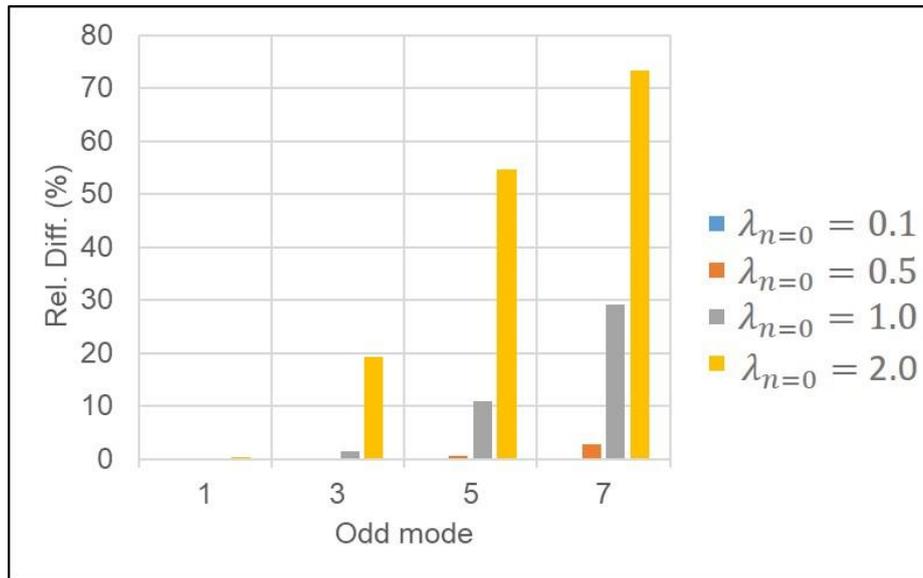
Fig. 6

Comparison of the relative differences between odd radial modes (odd values of m from 1 to 7) for several values of λ_0 ($\lambda_0 = \{0.1; 0.5; 1.0; 2.0\}$

3.4 Dynamic response

As a first step, the influence of the number of modes taken into account is studied for the analytical model in order to establish a reference "converged" model. This reference model is then compared with the FE model.

3.4.1 Influence of the number of modes

The influence of the number of modes is studied for the analytical model. The number of modes taken into account in the dynamic response is progressively increased for both directions independently.

Radial displacement must systematically contain a pair of symmetric modes. As explained in section 2.6.1, the radial displacement is positive for even values of n ($n = 2k$), whereas it is negative for odd values n ($n = 2k + 1$). Therefore, the dynamic response must contain the set of values for n composed of even values of n ($2k$) and its corresponding odd value ($n + 1$). It should be pointed out that this constraint does not apply to axial displacement.

The parameters analysed are the maximum and minimum displacements observed over the time range of the simulation. These parameters are considered since they are used to compute the DLF.

First, the analytical model is considered. Fig. 7 illustrates the variations in the relative difference applied to the maximum and minimum values of the radial displacement for the cylinder with $\lambda_0 = 0.1$. The reference displacement is considered with the first two symmetric modes (m is equal to 1 and 3).

$$Relative\ Difference(w) = \frac{Max(w) - Max(w, m = \{1,3\})}{Max(w, n = \{0,1\})}\ (\%)$$

The influence of the radial and axial modes on the radial displacement is successively analysed. A total of 16 radial modes are needed to observe stabilization in the results, whereas 6 axial modes are sufficient. The inflection of the radial displacement curve observed for 10 modes corresponds to the shift between the natural pulsations and their corresponding modes (either radial or axial modes).
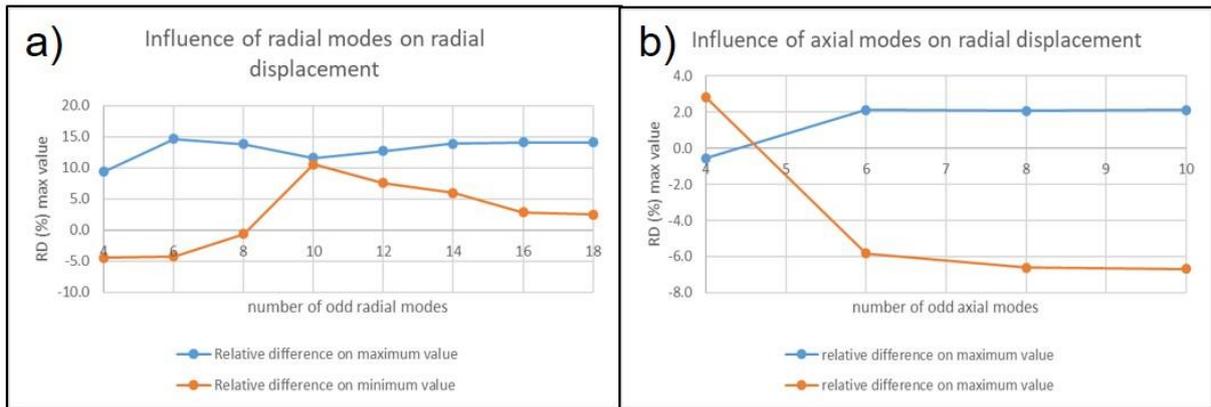
Fig. 7

Influence of the axial and radial modes on the radial displacement of the cylinder with $\lambda_0 = 0.1$ and with the analytical model – a) radial modes; b) axial modes

Fig. 8 presents the previous relative differences computed with the axial displacement. The results do not seem to stabilise with 16 radial modes, whereas only 8 axial modes are required. However, the variation is very low with 16 modes, which is why this number of radial modes is retained.
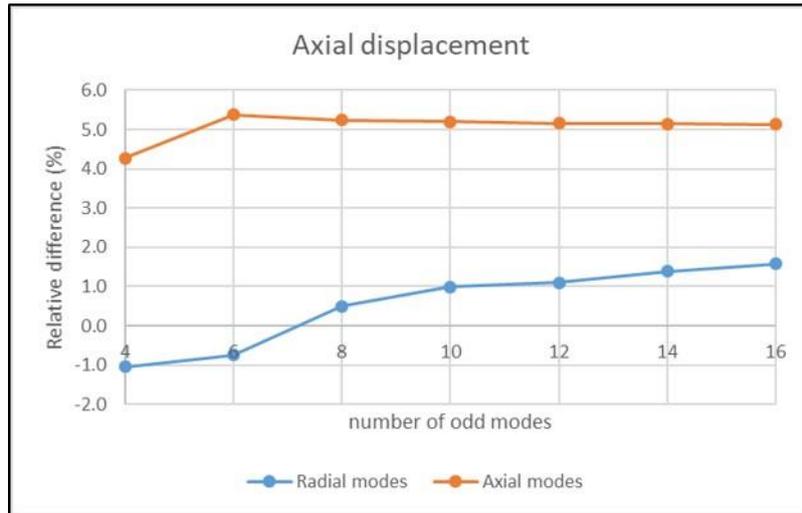
Fig. 8

Influence of the axial and radial modes on the axial displacement of the cylinder with $\lambda_0 = 0.1$ and with the analytical model

In conclusion, the first 16 radial modes and the first 8 axial modes are taken into account for the case with $\lambda_0 = 0.1$.

Similar analyses are performed for other values of λ_0. The results are summarised in table 7 (values for λ_0 are also recalled). The parameters for following parts are also given: the highest number of required modes are retained and applied to both displacements. A higher number of modes is required for the radial modes than for the axial modes.

	Radial displacement		Axial displacement		Applied parameters	
λ_0	Number of axisymmetric radial modes	Number of symmetric axial modes	Number of symmetric radial modes	Number of symmetric axial modes	Number of symmetric radial modes	Number of symmetric axial modes
0.1	16	8	16	6	16	8
0.5	10	4	16	4	16	4
1.0	12	4	14	4	14	4
2.0	8	4	14	4	14	4

Table 7: Number of modes taken into account in the dynamic response

3.4.2 Comparison with FE results

Fig. 9 presents the dynamic displacement response for radial and axial displacements, computed with both models (analytical dynamic model and FE model). Five graphs have been plotted for each value of λ_0. The first three curves concern the radial displacement and represent the dynamic displacement response, the maximum and minimum values (envelope) and the absolute difference between the FE and analytical responses. The remaining two curves concern the axial displacement with the displacement response and the absolute difference between FE and analytical responses.

For the lowest value of λ_0, both the radial and axial displacements are globally in good agreement with the FE results, especially at the beginning of the transient. However, differences appear in the radial displacements for t greater than 0.004 ms. Maximum and minimum values tend to be very close up to t of around 0.010 ms. With regard to the axial displacement, the curve plotting the difference between the response of the two models is

periodic at the beginning, following the response. The curve becomes slightly disrupted for t higher than 0.004 ms, and this difference increases. There are some differences between the two responses, which appear during the transient. These differences may be induced by either slight shifts in the frequencies or differences in the contribution of the modes. It should also be noted that the mean radius is considered in the analytical response, and in particular the effect of external forces (internal pressure) is computed with this value whereas pressure is applied to the internal radius for the FE model.

For λ_0 higher than 0.1, differences are observed earlier during the transient and they tend to be higher, especially for the radial direction. The radial displacement for the highest value of lambda (shortest cylinder) does not correspond between the two models.

These observations highlight the limit of the theory used (membrane theory), which correlate well for long cylinders. In addition, as previously explained, the internal pressure is applied to the inner radius for the FE model whereas it is applied to the mean radius for the analytical model. The DFT method provides further quantitative information to analyse the previous response and is presented in the next sub-section.
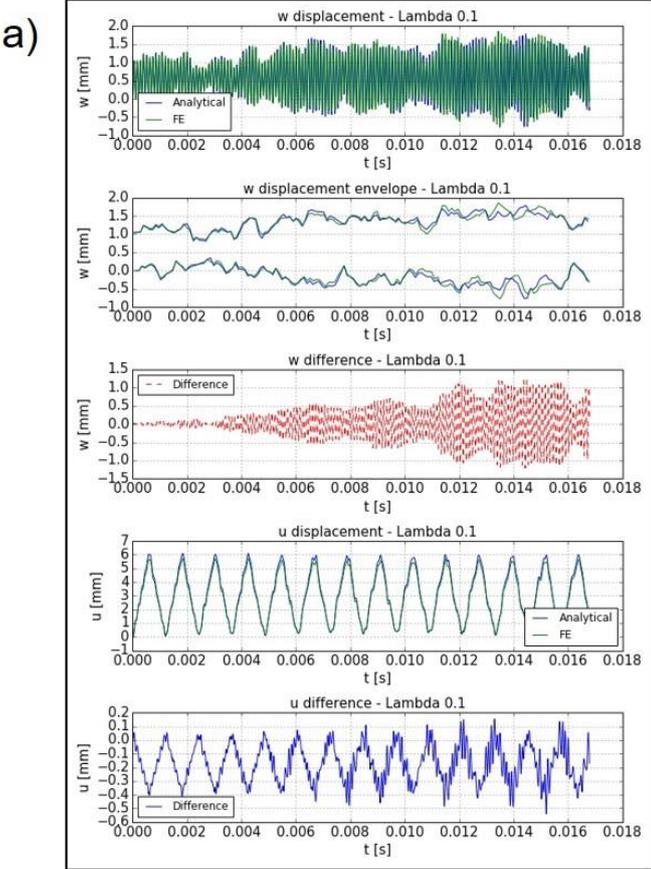
b)
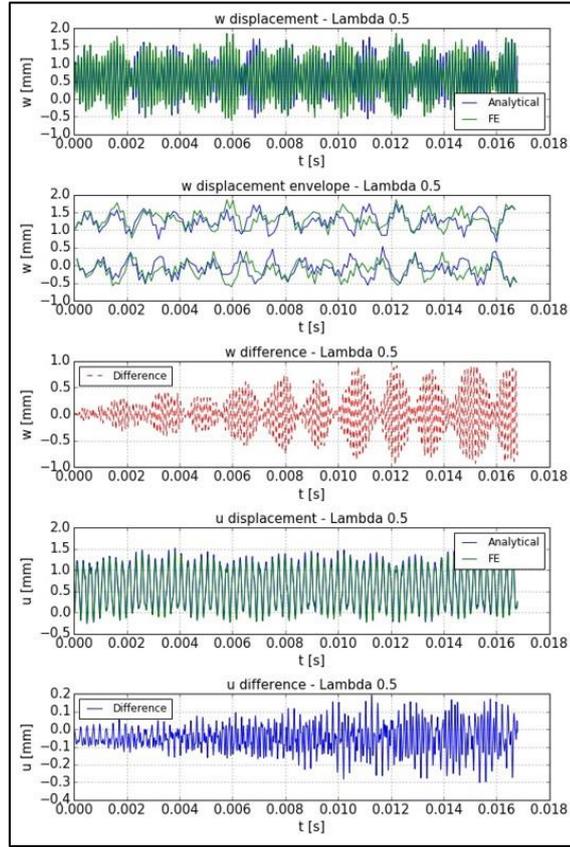
c)
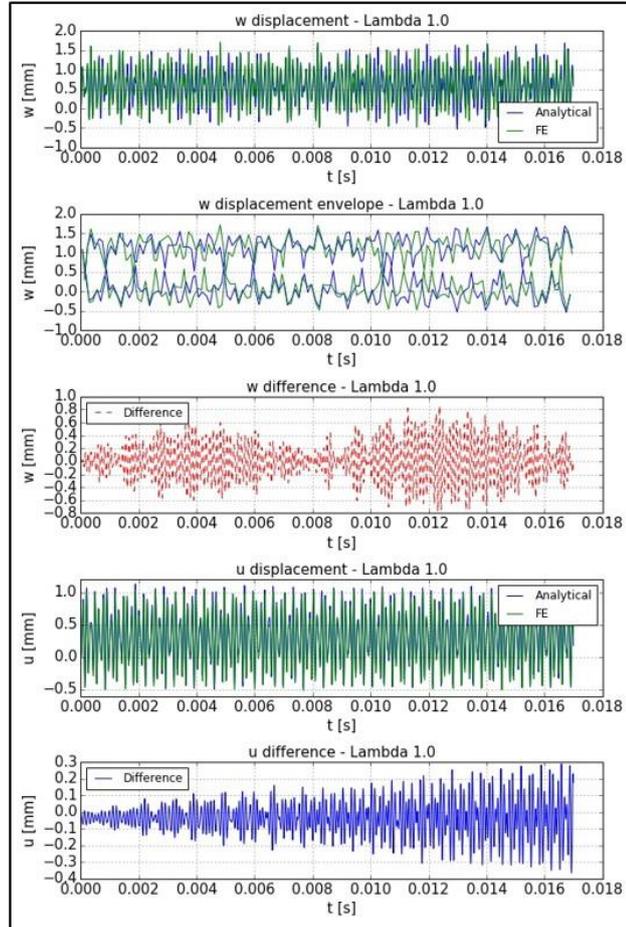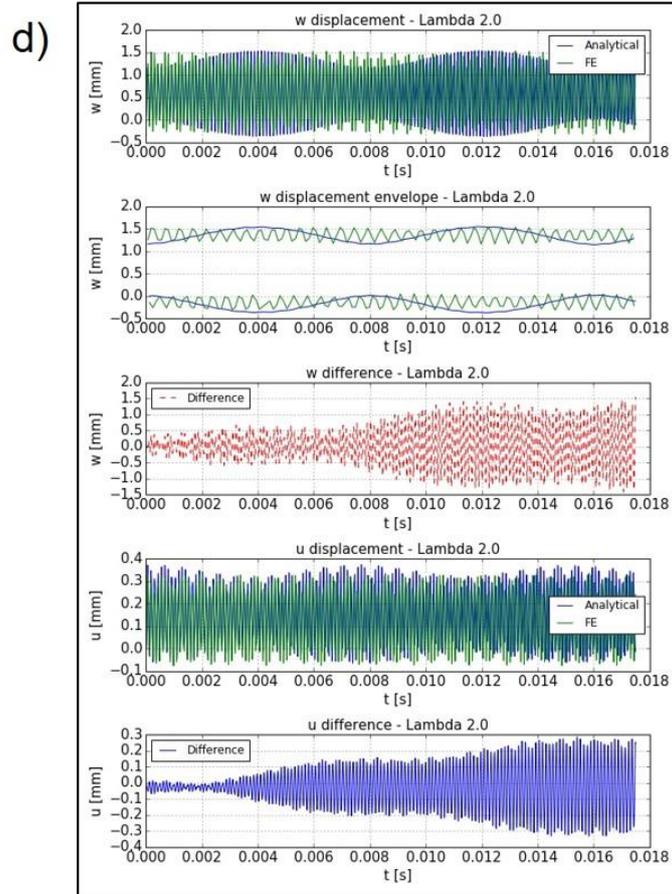
Fig. 9

Radial (w) and axial (u) displacements for several values of λ_0 – comparison between the analytical model and the FE model– a) $\lambda_0 = 0.1$; b) $\lambda_0 = 0.5$; c) $\lambda_0 = 1.0$; d) $\lambda_0 = 2.0$

3.5   DFT analysis

DFT spectra for both directions are shown in Fig. 10. Previous dynamic responses are compared (dynamic analytical model and FE simulations). This numerical method provides additional information compared with modal analysis: not only the frequency of the modes is provided, but also the contribution of these modes to the dynamic response. Both these parameters establish a "signature" of the dynamic response for each cylinder. This comparison should reflect the results observed for the DLF.

Detailed quantified results of the radial displacement and the axial displacement are presented in table 8 and table 9 respectively. The frequency and magnitude of the different main peaks are also indicated. Frequency values are compared with results of the modal analysis from section 3.3, which also provides the type of mode (axial or radial) and its number (odd values of m). f=0 corresponds to the "mean" value and contains the contributions of all modes.

First of all, the frequency values from DFT are in good agreement with the modal analysis, at least for the main frequencies (*i.e.* for the lowest values of m). Some harmonics cannot be retrieved. However, for the lowest values of λ_0 or when using the analytical model, the radial modes are so similar to each other that they cannot be discriminated with the applied DFT parameters. It should be remembered that the accuracy of the results depends on the DFT parameters (number of samples and time step). Conclusions are similar to those from the modal analysis (section 3.3): the main radial mode frequencies correlate well between the two models for long cylinders. They are in very good agreement for axial displacements whatever the shape of the cylinder.

The mean value (f=0) and the two fundamental modes (in bold in the tables) are compared to better understand the magnitude of the peaks. Mean values are globally constant with λ_0 for radial displacements whereas they decrease for axial displacements (shorter cylinders result in lower axial displacement). With regard to the radial

direction, the results are in very good agreement between the two models, even if differences seem to increase slightly for $\lambda_0 = 2.0$. Moreover, the highest differences can be observed for radial modes whereas axial mode contributions are relatively similar between the two models. These observations are probably due to the difference in the modal behaviour along the radial direction, as shown in section 3.3. However, DFT analysis suggests that harmonic radial modes reveal differences not only in their frequencies but also in the extent of their contribution.

Differences with regard to the axial direction tend to be higher than for the radial direction and seem to increase with λ_0. The same conclusions as for radial displacements can be applied to axial displacements. In addition, the mean displacement (f=0) seems to be over-estimated by the analytical model. In addition, for $\lambda_0 \geq 1.0$, the main contribution corresponds to a radial mode whereas it is an axial mode for $\lambda_0 \leq 1.0$.

In conclusion, DFT is an efficient tool for characterizing and comparing the response of the cylinder. It can be used to identify the main frequencies contributing to the response and their relative impact. The results show good agreement for the radial displacement when considering the mean value (f=0) and the two fundamental modes. Differences are slightly higher for the axial displacement, even for the mean value (f=0). Spectra are especially similar for the lowest value of λ_0 even if slight differences can be observed, which should partially explain the difference observed with the dynamic response. The differences tend to be slightly more pronounced for higher values of λ_0. This is probably due to the shift in frequencies for the harmonic radial modes between the analytical and FE models. However, DFT suggests that there is also a difference in the magnitude of the contribution for these modes.

The DFT results could be improved with more appropriate parameters (reduce of Δf) but this would require increasing the quantity of data.

b)

DFT - w displacement - Lambda 0.5

Analytical
FE

w [mm]

f [Hz]

DFT - u displacement - Lambda 0.5

Analytical
FE

u [mm]

f [Hz]

c)

DFT - w displacement - Lambda 1.0

Analytical
FE

w [mm]

f [Hz]

DFT - u displacement - Lambda 1.0

Analytical
FE

u [mm]

f [Hz]
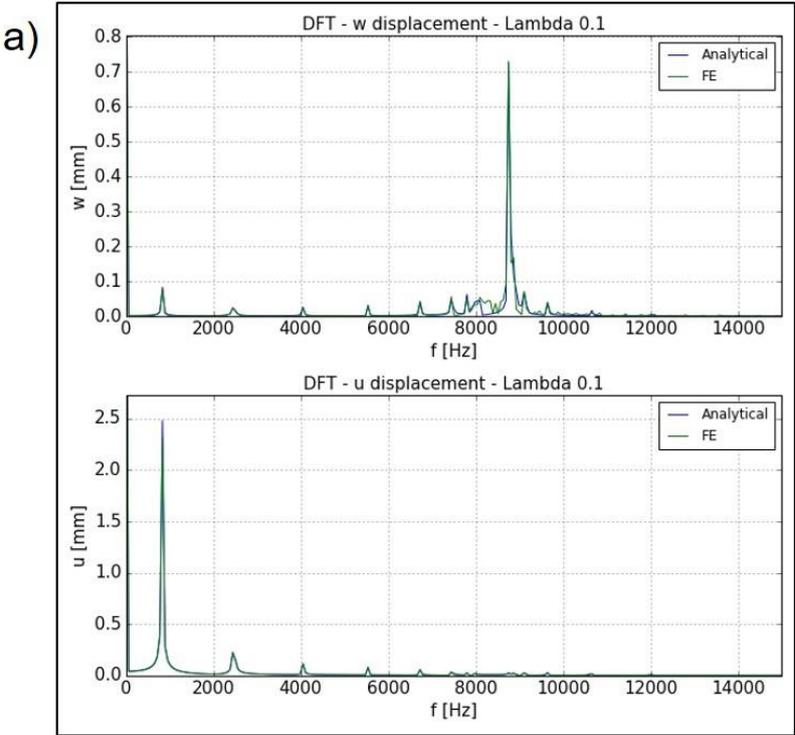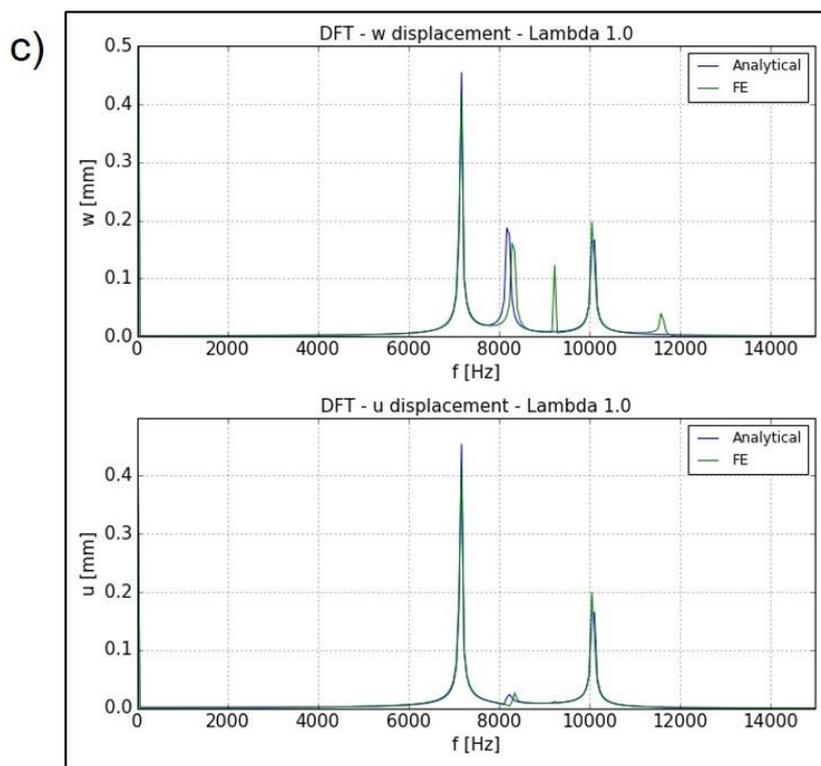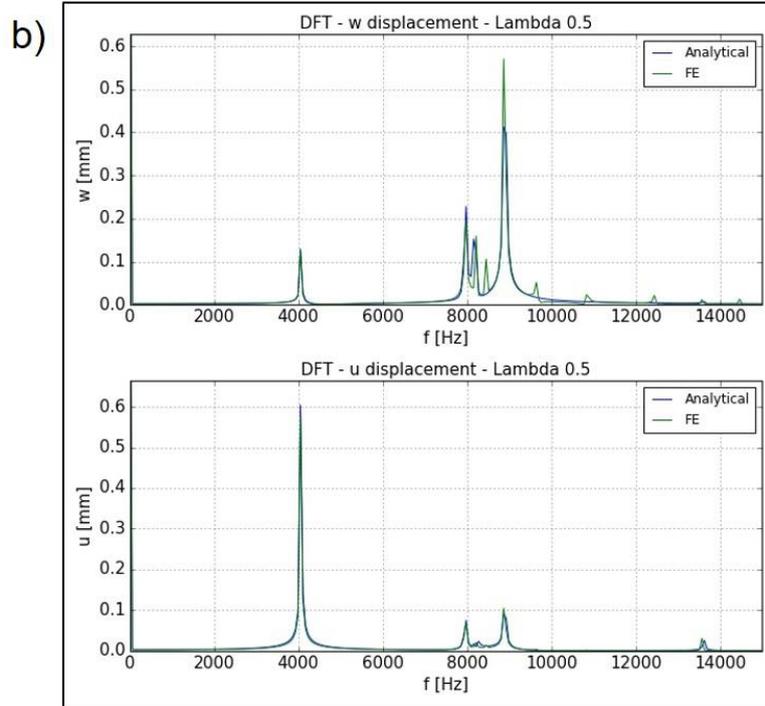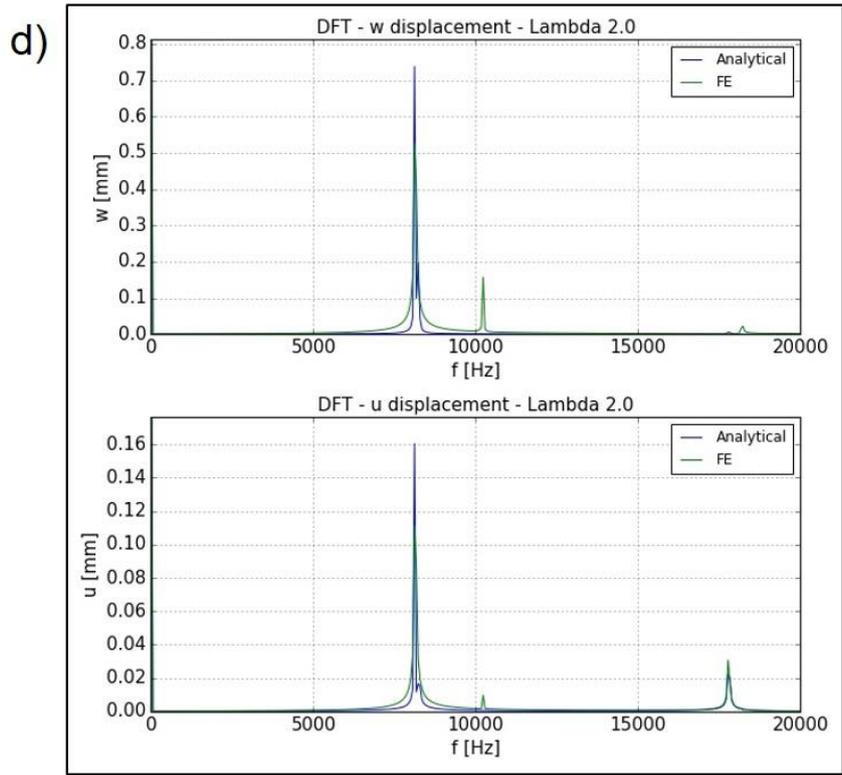
Fig. 10

DFT of displacements for several values of λ_0 – comparison between the analytical model and the FE model – a) $\lambda_0 = 0.1$; b) $\lambda_0 = 0.5$; c) $\lambda_0 = 1.0$; d) $\lambda_0 = 2.0$

λ_0	m R/A	**Analytical model**			**FE model**			DFT parameter	Relative difference on magnitude
		Modal analysis	DFT		Modal analysis	DFT			
		f	f	Magnitude	f	f	Magnitude	Δf	
		Hz	Hz	mm	Hz	Hz	mm	Hz	%
0.1	-	-	**0**	**1.185**	-	**0**	**1.182**	59.5	**-0.3**
	1/A	**825**	**834**	**0.083**	**825**	**834**	**0.076**		**9**
	3/A	2465	2441	0.025	2464	2441	0.024		4
	5/A	4060	4048	0.027	4060	4048	0.023		17
	1/R	**8754**	**8752**	**0.727**	**8759**	**8752**	**0.730**		**-0.4**
	3/R	8795	-	-	8800	-	-		
	5/R	8899	-	-	8904	8871	0.169		
	7/R	9130	9109	0.072	9134	9109	0.067		7
0.5	-	-	**0**	**1.185**	-	**0**	**1.179**	60.1	**0.5**
	1/A	**4060**	**4087**	**0.095**	**4060**	**4087**	**0.089**		**7**
	3/A	13617	13643	0.008	13617	13583	0.007		14
	1/R	**8899**	**8895**	**0.630**	**8904**	**8895**	**0.680**		**-7**
	3/R	7960	7933	0.177	7965	7993	0.153		16
	5/R	8176	8174	0.181	8233	8234	0.155		17
1.0	-	-	**0**	**1.181**	-	**0**	**1.178**	60.1	**0.3**
	1/A	**10090**	**10097**	**0.250**	**10090**	**10097**	**0.254**		**-2**
	3/A	26422	26443	0.001	26413	27405	0.004		-75
	1/R	**7161**	**7152**	**0.489**	**7162**	**7152**	**0.470**		**4**
	3/R	8204	-	-	8329	8354	0.174		
	5/R	8240	8234	0.189	9245	9255	0.093		103
2.0	-	-	**0**	**1.181**	-	**0**	**1.219**	60.1	**-3**
	1/A	**17799**	**17789**	**0.007**	**17797**	**17789**	**0.007**		**0**
	1/R	**8119**	**8113**	**0.736**	**8140**	**8113**	**0.523**		**40**
	3/R	8246	8233	0.215	10224	10217	0.152		41

Table 8: DFT results for the radial displacement ($w(z = L/2)$)

λ_0	m R/A	**Analytical model**			**FE model**			DFT parameter	Relative difference on magnitude
		Modal analysis	DFT		Modal analysis	DFT			
		f	f	Magnitude	f	f	Magnitude	Δf	%
		Hz	Hz	mm	Hz	Hz	mm	Hz	
0.1	-	-	**0**	**6.250**	-	**0**	**5.838**	59.5	**7**
	1/A	**825**	**834**	**2.481**	**825**	**834**	**2.311**		**7**
	3/A	2465	2441	0.227	2464	2441	0.215		6
	5/A	4060	4048	0.118	4060	4048	0.114		4
	1/R	**8754**	**8752**	**0.026**	**8759**	**8752**	**0.021**		**24**
	3/R	8795	-	-	8800	-	-		
	5/R	8899	8871	0.021	8904	8871	0.023		-9
	7/R	9130	9109	0.026	9134	9109	0.029		-10
0.5	-	-	**0**	**1.240**	-	**0**	**1.131**	60.1	**9**
	1/A	**4060**	**4087**	**0.447**	**4060**	**4087**	**0.418**		**7**
	3/A	13617	13643	0.019	13617	13583	0.025		-24
	1/R	**8899**	**8895**	**0.134**	**8904**	**8895**	**0.125**		**7**
	3/R	7960	7933	0.057	7965	7993	0.058		-2
	5/R	8176	-	-	8233	8234	0.025		
1.0	**-**	**-**	**0**	**0.616**	**-**	**0**	**0.545**	60.1	**13**
	1/A	**10090**	**10097**	**0.253**	**10090**	**10097**	**0.254**		**-0.4**
	3/A	26422	26443	0.002	26413	26383	0.004		-50
	1/R	**7161**	**7152**	**0.492**	**7162**	**7152**	**0.473**		**4**
	3/R	8204	8173	0.020	8329	8354	0.023		-13
	5/R	8240	8294	0.017	9245	9255	0.009		89
2.0	-	-	**0**	**0.309**	-	**0**	**0.254**	60.1	**22**
	1/A	**17799**	**17789**	**0.032**	**17797**	**17789**	**0.038**		**-16**
	1/R	**8119**	**8113**	**0.16**	**8140**	**8113**	**0.111**		**44**
	3/R	8246	8233	0.017	10224	10217	0.01		70

Table 9: DFT results for the axial displacement ($u(z = 0)$)

3.6 DLF analysis

In this subsection, the DLF values of the global response (*i.e.* taking into account several or all modes) are computed for the four previous cylinders. These values can be obtained using the analytical relations established in section 2.6. They can also be evaluated directly by using the maximum value from the dynamic response (*i.e.* temporal response presented in section 3.4) obtained either with the dynamic analytical model or with the previous FE model. The results are presented and compared in the following subsections.

3.6.1 DLF using analytical relations

The DLF values are calculated using the analytical relations given in section 2.6. It should be remembered that these relations are derived from the dynamic analytical equations using conservative simplifications. Two methods are considered to combine the modes: the sum method and the RMS method. The results obtained with both methods are compared in this section. The specific values corresponding to the four considered cylinders are indicated. When the exact result is not known, the sum is approximated by taking into account the maximum number of symmetric modes deduced from the analysis presented in subsection 3.4.1 (truncation of the series): the first 16 modes are selected. Concerning the radial DLF, only half of the 16 modes must be considered since only even values of n are retained to compute the DLF (see subsection 2.6.1, positive displacement).

All the results are shown in table 10 for the radial direction and in table 11 for the axial direction. Fig. 11 presents the variations in the axial DLF computed with the different established relations.

The results with the two methods are different. The RMS method is systemically lower with a relative difference from around -10 % to -35 %. Concerning the axial direction, differences tend to be rather low between the two considered conservative approximations ($DLF\left(u, \lambda_n = (2\,n + 1)\right)$ and $DLF(u, \lambda_n = 1)$). The relative difference between the second approximation ($DLF(u, \lambda_n = 1)$) and the first approximation ($DLF\left(u, \lambda_n = (2\,n + 1)\right)$) is 9 % with the sum method and less than 0.1 % with the RMS method. Fig. 11 confirms that the axial DLF computed with the full expression reaches a maximum value for $\lambda_0 = 1$.

$DLF_{sum}(w)$	Reference of equation	Equation (25)
	Approximation with the first 8 terms	4.01
$DLF_{RMS}(w)$	Reference of equation	Equation(26)
	Approximation with the first 8 terms	$2.63\ (\leq \frac{4}{\sqrt{2}} \approx 2.83)$
Relative difference (RMS vs sum)		-35 %

Table 10: Global radial DLF from analytical model

		Full expression	First conservative approximation $\lambda_0 = 1$	Second conservative approximation $\lambda_n = 1 \, \forall \, n$
$DLF_{sum}(u)$	Reference of equation	Equation (27) $DLF_{sum}(u)$	Equation (28) $DLF_{sum}(u, \lambda_n = (2\,n+1))$	Equation (29) $DLF_{sum}(u, \lambda_n = 1) = \dfrac{(1+\nu)}{\nu}$
	Approximation with the first 16 terms	See Fig. 11 Depends on λ_0 <table><tr><td>λ_0</td><td>$DLF(u)$</td></tr><tr><td>0.1</td><td>2.09</td></tr><tr><td>0.5</td><td>2.51</td></tr><tr><td>1.0</td><td>3.64</td></tr><tr><td>2.0</td><td>2.41</td></tr></table>	3.64 $(\geq \frac{24}{\pi^2})$	$3.98 \leq \dfrac{(1+\nu)}{\nu} \approx 4.03$
$DLF_{RMS}(u)$	Reference of equation	Equation (30) $DLF_{RMS}(u)$	Equation (31) $DLF_{RMS}(u, \lambda_n = (2\,n+1))$	Equation (32) $DLF_{RMS}(u, \lambda_n = 1)$ $= \dfrac{2}{\sqrt{6}} \dfrac{(1+\nu)}{\nu}$
	Approximation with the first 16 terms	See Fig. 11 Depends on λ_0 <table><tr><td>λ_0</td><td>$DLF(u)$</td></tr><tr><td>0.1</td><td>1.65</td></tr><tr><td>0.5</td><td>2.07</td></tr><tr><td>1.0</td><td>3.27</td></tr><tr><td>2.0</td><td>2.06</td></tr></table>	3.27 $(\geq \frac{24}{\pi^2})$	$3.29 \approx \dfrac{2}{\sqrt{6}} \dfrac{(1+\nu)}{\nu}$
Relative difference (RMS vs sum)		<table><tr><td>λ_0</td><td>$DLF(u)$</td></tr><tr><td>0.1</td><td>-21 %</td></tr><tr><td>0.5</td><td>-18 %</td></tr><tr><td>1.0</td><td>-10 %</td></tr><tr><td>2.0</td><td>-15 %</td></tr></table>	-10 %	-17 %

*Table 11: Global axial DLF from analytical model*
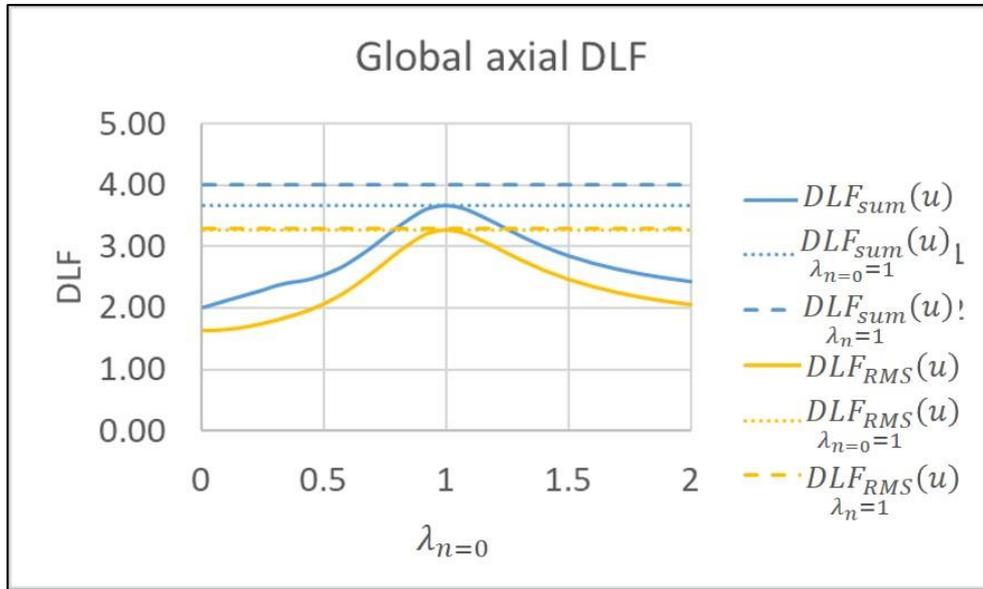
Fig. 11

Global axial DLF with the different methods based on analytical model ($\nu = 0.33$)

3.6.2 DLF from dynamic response and comparison

In this subsection, global DLF are computed from the dynamic response, which was obtained either from the analytical model or from the FE simulations. The maximum displacements of the dynamic response (see subsection 3.4 for the model set-up and the parameters) are established. The DLF can then be calculated by using the previous static displacements (see subsection 3.2). Finally, all the results are compared with those obtained using the analytical relations from subsection 3.6.1.

When computing the maximum displacements of the dynamic response, the time corresponding to this maximum cannot be predicted *a priori*. Therefore, the dynamic response should be computed for any time, which is obviously impossible. For the dynamic response, the number of cycles taken into account is indicated. It is computed on basis of the lowest frequency of the different modes considered with the analytical model.

The different results for the global DLF (analytical relations and dynamic response using the analytical model) are compared with the value computed with the FE dynamic response with the relation: relative difference=$\frac{(DLF - DLF_{FE})}{DLF_{FE}}$ (%).

Tables 12 and 13 present the results for the radial and axial DLF respectively.

First, the values computed with the dynamic response (itself obtained with the analytical model) are very close to those obtained with the FE model: the maximum absolute relative difference is 9 %. Even if the analytical dynamic response presents some differences with the FE model, the impact is negligible on the DLF estimation. Most of the cases underestimate the DLF when the analytical model is used (*i.e.* DFL with analytical dynamic model < DLF with FE model).

The following observations can be made with respect to estimating the DLF using the different methods and equations established on basis of the analytical model. With regard to the **radial direction**, the sum function is always conservative as expected (*i.e.* the DLF is higher than the actual value obtained with the dynamic response), whereas the RMS function is generally not conservative except for one case (shortest cylinder). The latter should not be used for design purposes. The sum function presents relatively high differences with the dynamic response (either with analytical or FE models). As previously explained, the time of the maximum response is not known, so that maximum value obtained with the dynamic response cannot be set as a reference. The most conservative value obtained with the sum function is around 4.01, which is much higher than the regular value of 2.0 obtained with a SDOF model. Differences between the DLF obtained with the dynamic responses are low, and seem to decrease with λ_0. The DLF analysis in section 3.5 concluded that the mean displacement and the fundamental mode contributions are in good agreement, whereas differences are higher for harmonics. This suggests that the mean displacement and the fundamental modes are the main contributors to the DLF value and are correctly represented with the analytical model from the DLF point of view.

Concerning the **axial direction**, the sum method with the most conservative approximation is always conservative as expected. The relative difference may be very high, up to 102 %, but this relation does not take into account the shape of the cylinder. For $\lambda_0 = 1$, difference is negligible (2%). Less conservative models reduce the difference, but they can underestimate the DLF on the other hand. The sum function using the full expression is the closest to the actual (*i.e.* FE) results (the maximum absolute relative difference is 7 %). Concerning the DLF computed with the RMS function, values are not systematically conservative, even if estimations are improved with the most conservative approximation ($DLF_{RMS}(u, \lambda_n = 1)$). As previously proved for the radial direction, the RMS method should not be used for design. Differences between the dynamic responses are low and seem to increase with λ_0, as was concluded with the DLF analysis. The same conclusions as for dynamic radial displacement can be applied for axial displacement: the mean displacement and the fundamental modes are the main contributors to the DLF value and are correctly represented with the analytical model from a DLF perspective.

As a conclusion, the relation using the sum of all the DLF with the most conservative approximation (*i.e.* $DLF_{sum}(u, \lambda_n = 1)$) can be used for design as it always provides conservative values. The relation is very simple and it avoids computing the dynamic response of the system, which is more complex and cannot guarantee the conservatism of the result. However, this relation does not take into account the effect of geometry and consequently can be highly conservative for values of λ_0 that are far from 1.0. In this case, the second relation using the less conservative approximation ($DLF_{RMS}(u, \lambda_n = (2n + 1))$) can be used as it slightly reduces the difference. As for radial direction, the maximum DLF value is much higher than 2.0. (up to nearly 4.0).

		λ_0			
		0.1	0.5	1.0	2.0
Analytical model	$DLF_{sum}(w)$	4.01			
	Relative difference	26 %	25 %	38 %	59 %
	$DLF_{RMS}(w)$	2.63			
	Relative difference	-17 %	-18 %	-9 %	4 %
	From dynamic response	3.02	2.90	2.79	2.55
	Relative difference	-5 %	-9 %	-4 %	1 %
FE	From dynamic response	3.18	3.20	2.90	2.52
Number of cycles (FE & analytical)		13863	68776	169446	135098

Table 12: DLF - radial displacement ($w(z = L/2)$)

			λ_0			
			0.1	0.5	1.0	2.0
Analytical model	Analytical relations with the sum function	$DLF_{sum}(u)$	2.09	2.51	3.64	2.41
		Relative difference	6 %	-0.4 %	-6 %	-7 %
		$DLF_{sum}(u, \lambda_n = (2\,n+1))$	3.64			
		Relative difference	85 %	44 %	-6 %	41 %
		$DLF_{sum}(u, \lambda_n = 1)$	3.98			
		Relative difference	102 %	58 %	2 %	54 %
	Analytical relations with the RMS function	$DLF_{RMS}(u)$	1.65	2.07	3.27	2.06
		Relative difference	-16 %	-18 %	-16 %	-20 %
		$DLF_{RMS}(u, \lambda_n = (2\,n+1))$	3.27			
		Relative difference	66 %	30 %	-16 %	26 %
	Explicit dynamic response	From dynamic response	1.96	2.43	3.62	2.39
		Relative difference	-1 %	-4 %	-7 %	-8 %
FE		From dynamic response	1.97	2.52	3.89	2.59
Number of cycles (FE & analytical)			13863	68776	169446	135098

Table 13: DLF - axial displacement ($u(z = 0)$)

4 Conclusion

This paper addresses the issue of designing a cylindrical test section subjected to a dynamic internal pressure for severe accident experiments. A commonly used method consists in computing the static equivalent response of the structure and then applying DLF coefficients. DLF coefficients are therefore obtained for cylinders in this paper.

To do this, a coupled MDOF analytical model of the cylinder subjected to a stepped internal pressure is set up. This model is based on modal response. The associated maximum DLF of the cylinder is estimated for both radial and axial displacements for each mode and finally for the global response. It has been found that the axial DLF reaches a maximum for the specific value $\lambda_0 = \frac{\pi R}{L}$, while the radial DLF does not depend on the geometry. Conservative values have been established using very simple formulas and without computing the dynamic response of the cylinder. However, as the geometry (parameter λ_0) is not taken into account, differences (*i.e.* conservatism) can be high for some cases. These differences can be reduced, but this requires more complex relations, even if they are less cumbersome than computing the dynamic response. The sum method is recommended compared with the RMS method for design, as conservative values are always obtained, especially when using the second approximation for axial displacement ($DLF(u, \lambda_n = 1)$).

The results have been compared with FE simulations. For long cylinders (*i.e.* $\lambda_0 \leq 0.1$), the dynamic results are globally validated, as are the DLF computed from the dynamic response. However, the difference for the axial DLF increases with the increase in λ_0 (shorter cylinders), contrary to radial DLF. Nevertheless, the impact on DLF is low: the maximum relative difference is 9 %. DFT comparisons of both dynamic responses shows that the two models share very similar results for the mean displacement and for the fundamental mode of both radial and axial displacements. This result suggests that these parameters are the main characteristic values to consider from a DLF point of view.

When the radial and axial modes are coupled, the regular value of 2.0 established for SDOF model is exceeded. The difference can be significantly higher (DLF up to 4.0 with analytical model, 3.9 with FE but for a finite range of time).

The membrane theory has been applied. It essentially neglects the bending moments. Therefore, some differences appear in the dynamic response, which increase as λ_0 increases. The actual radial harmonic modes shift from the frequencies given with the analytical model. The results may be improved by taking into account these moments, as done in Chengyi *et al.* (1996). A model is also proposed in [11] for axisymmetric loading. Results should not only depend on the ratio R/L but also on the thickness. However, the resulting analytical equations would be more sophisticated.

The cylinder is simply supported and considered to be open-ended, which does not correspond to the usual configuration of a pressurized vessel. This model can be extended to closed cylinders. Preliminary analyses have shown different results from those presented in this paper. Regular boundary conditions (*e.g.* one extremity fixed while the other is free) are more difficult to solve. The model can also be easily extended to other simple typical loads, which can be modelled with classical mathematical functions (such as triangular or exponential loads).

The results should be assessed with dedicated experiments. However, the cylinder response depends on both the boundary conditions and the applied loading. Previous boundary conditions cannot be easily reproduced experimentally. The model will need to be modified. The other point concerns the loading, which will not correspond to the ideal load applied to the previous models. Therefore, it should be dynamically characterized as well as its spatial distribution thanks to different sensors. Finally, structural damping may also affect the dynamic response of the actual structure, which is not taken into account for the model.

5   Declarations

Conflicts of interest/Competing interests:

The authors have no financial or proprietary interests in any material discussed in this article.

Availability of data and material:

The datasets generated and analysed during the current study are available from the corresponding author on reasonable request.

Code availability:

Cast3M has been used and is available on Cast3M website (http://www-cast3m.cea.fr).

Authors' contributions:

Christophe Garnier: methodology, original draft, writing and editing

Vincent Faucher: review and proof reading

Pierre Lamagnère: review and proof reading

7 References

1. Journeau, C., Buffe, L., Haquet, J.-F., Piluso, P., Willermoz, G. (2015). Needs for large mass prototypic corium experiments the PLINIUS-2 platform, NURETH 2015 – 16th International Topical Meeting on Nuclear Reactor Thermal Hydraulics, Aug 2015, Chicago, United States.

2. Serre, F., Payot, F., Suteau, C., Journeau, C., Aufore, L. *et al.* (2017). Plinius-2 a new corium facility and programs to support the safety demonstration of the ASTRID mitigation provisions under severe accident conditions, International Conference on Fast Reactors and Related Fuel Cycles Next Generation Nuclear Systems for Sustainable Development (FR17), Jun 2017, Lekaterinbourg, Russia.

3. Biggs, J.M. (1964). Introduction to structural dynamics, McGraw-Hill Companies.

4. Mindlin, R. D., Bleich, H. H. (1953). Response of an elastic cylindrical shell to a transverse step shock wave, Journal of Applied Mechanics, Vol. 20, No. 2, pp. 189-195.

5. Haywood, R. W (1958). Response of an elastic cylindrical shell to a pressure pulse, Quaterly Journal of Mechanics and Applied Mathematics, Vol. 11, No. 2, pp 129- 141.

6. Herman, H., Klosner, J. M. (1965). Transient response of a periodically supported cylindrical shell immersed in a fluid medium, Journal of Applied Mechanics, Vol. 32, No. 3, pp. 562-568.

7. Humphreys, J. S., Winter, R. (1965). Dynamic response of a cylinder to a side pressure pulse, AIAA Journal, Vol. 3, No. 1.

8. Costantino, C.J. (1965). The Strength of Thin-Walled Cylinders Subjected to Dynamic Internal Pressures, Journal of Applied Mechanics, Vol. 32, No. 1, pp. 104-108.

9. Geers, T. L (1969). Excitation of an elastic cylindrical shell by a transient acoustic wave, Journal of Applied Mechanics, pp. 459-469.

10. Islam, M.N., Kormi, K., Al-Hassani, S.T.S. (1992). Dynamic response of a thin-walled cylinder to side pressure pulse, Engineering Structures, Vol. 14, No. 6, pp. 395-412.

11. Markuš, Š. (1988). The mechanics of vibrations of cylindrical Shells.

12. Mushtari, Kh. M. (1938). Certain generalization of the theory of thin shells, Izv. Fiz.-Mat. Ob-va pri Kazanskom Universitete, Vol. 11, No. 8.

13. Donnell, L. H. (1938). A discussion of thin shell theory, Proceedings of the 5th international Congress of Applied Mechanics, John Wiley, New York, pp. 66-70.

14. Love, A. E. H. (1944). A treatise on the mathematical theory of elasticity, Dover Publications, New York.

15. Timoshenko, S. (1959). Theory of plates and shells, McGraw-Hill, New York.

16. Flügge, W. (1962). Stress in shells, Springer-Verlag, Berlin.

17. Hwang, E-S., Nowak, A. S. (1991). Simulation of Dynamic Load for Bridges, Journal of Structural Engineering, Vol. 117, No. 5, pp. 1413-1434.

18. Pernica, G. (1990). Dynamic Load Factors for pedestrian movements and rythmic exercices, Canadian Acoustics, Vol. 18, No. 2, pp. 3-18.

19. Morrison, C. M. (2006). Dynamic response of walls and slabs by single-degree-of-freedom analysis-a critical review and revision, International Journal of Impact Engineering, Vol. 32.

20. Dong, Q. Hu, B. Y., Chen, S.Y., Gu, Y. (2012). Engineering Design of a Multiple-Use Spherical Explosion Containment Vessel Subjected to Internal Blast Loading From 25 kg TNT High Explosive, Journal of Pressure Vessel Technology, 2012.

21. Chen, Y., Zheng, J., Deng, G., Ma, Y., Sun, G. (2008). Methods for design of explosion containment vessels, Proceedings of PVP 2008, Volume 1, Codes and Standards, pp. 489-502.

22. Oswald, C.J., Polcyn, M.A., Esparza, E.D. (1994). Dynamic design and proof testing of blast containment vessel, PVP vol. 272, Sloshing, fluid structure interaction and structural response due to shock and impact loads, ASME 1994.

23. Chengyi, H., Tuguang, L., Jijia Z. (1996). Elastic pulse buckling of cylindrical shells under radial impulsive loading, Applied Mathematics and Mechanics, English edition, Vol. 17, No. 8, pp 781-788.

24. De Malherbe, M. C., Wing, R. D., Laderman, A. J., Oppenheim, A. K. (1966). Response of a cylindrical shell to internal blast loading, Journal of Mechanical Engineering Science, Vol. 8, No. 1, pp. 91-98.

25. Beltman, W. M., Shepherd, J.E. (2002). Linear elastic response of tubes to internal detonation loading, Journal of Sound and Vibration, Vol. 252, No. 4, pp. 617-655.

26. Mirzaei, M. (2008). On amplification of stress waves in cylindrical tubes under internal dynamic pressure, International Journal of Mechanical Sciences, Vol. 50, pp. 1292-1303.

27. Cast3M software, 2018 release. Cast3M website: http://www-cast3m.cea.fr (release 20.01.1), accessed 15 March 2021.

28. SciPy.org, NumPy v1.11 Manual, NumPy Reference, Routines, Discrete Fourier Transform (numpy.fft). https://docs.scipy.org/doc/numpy-1.11.0/reference/routines.fft.html (accessed 23 November 2020).

29. Young, W. C., Budynas, R. G. (2002). Roark's formulas for stress and strain, seventh edition, McGraw-Hill.